Timing and distribution of bedding-parallel veins, in evaporitic rocks, Bouhedma Formation, Northern Chotts, Tunisia

Nabil Abaab, Alain Zanella, Dhaou Akrout, Régis Mourgues, Mabrouk Montacer

Timing and distribution of bedding-parallel veins, in evaporitic rocks, Bouhedma Formation, Northern Chotts, Tunisia.

Nabil ABAAB[a, b, c *], Alain ZANELLA[b], Dhaou AKROUT [a, d], Régis MOURGUES[b] , Mabrouk MONTACER[a]

[a] U.R : 3G - Géosystèmes, Géoressources et Géoenvironnements, UR13ES80, Faculté des Sciences de Gabès, Tunisie

[b] Le Mans Université, Géosciences Le Mans - LPG UMR 6112, 72085, Le Mans, France

[c] Institut Supérieur des Sciences et Techniques des Eaux de Gabès, Université de Gabès, Gabès, Tunisia ;

[d] École Supérieure polytechniques, 4303 Cité Cadres, Sebkha Nouakchott, Mauritanie ;

*Corresponding author:

ABAAB Nabil*

Email address: nabil.abaab.etu@univ-lemans.fr.

Le Mans Université, Géosciences Le Mans - LPG UMR 6112, 72085, Le Mans, France

Abstract

Bedding-parallel veins, 'BPV', are widespread worldwide especially within sediments of low permeability such as mudstones, marls and evaporitic formations. Gypsum, calcite or quartz fibrous minerals compose these geological features as well as less common components such as bitumen. These structures are heavily studied as they provide significant information about the paleo-stress states, host rock deformation and fluid flow. In the Bouhedma Formation, Northern Chotts Range, Southern Tunisia, although gypsum BPV are clearly observed there is particularly a dearth of published data concerning their characterization. Petrographic examination, tectonic and micro-tectonic analysis of both of the BPV and host rocks were conducted to determine their origin and the formation mechanism of the bedding-parallel fibrous gypsum veins in the Bouhedma Formation.

Field studies indicate that the host rocks for the BPV are mostly mudstones and evaporites. The BPV are especially localized within the lower part of the Bouhedma Formation, at boundaries between these sedimentary beds. The deformed gypsum and anhydrite fibers composing the BPV indicate vein growth during the shortening of the basin from the Miocene through Villafranchian times. We argue that the BPV are the result of fluid overpressure and natural hydraulic fracturing in low-permeable sediments due to mineralogical transformations and tectonic compression.

Key words: Bedding parallel veins, "beef", gypsum, fluid overpressures, lower Cretaceous, Tunisia.

1. Introduction

Natural hydraulic fractures are common in sedimentary basins worldwide, especially within strata of low-permeability (Cobbold et al., 2013; Gale et al., 2014; Zanella et al., 2020). In many cases, bedding-parallel veins 'BPV', also called 'beef veins' (Buckland & De la Bèche, 1835), represent this natural hydraulic fracture process (Philipp, 2008). The BPV are known to be composed of fibrous minerals containing either quartz, calcite or gypsum for the most common ones (Cobbold et al., 2013). Given their role in the potential fluid redistribution in sedimentary basins, the BPV have been heavily studied during the last two decades, especially those of calcite composition in basins related to hydrocarbon resources (e.g. Rodrigues et al., 2009; Meng et al., 2017a; Weger et al., 2018; Ukar et al., 2020), and those of gypsum composition especially in evaporitic sediments (Shearman et al., 1972; Machel, 1985; Gustavson et al., 1994; El Tabakh et al., 1998; Cosgrove, 2001; Philipp, 2008; Cobbold et al., 2013; Rustichelli et al., 2016; Meng et al., 2017b, 2017c, 2019).

Veins are categorized into three kinds based on the direction of crystal growth, crystal shape, and the number of growth generation: stretched vein, syntaxial vein, and antitaxial vein (Durney and Ramsay, 1973; Bons and Montenari, 2005; Bons et al., 2012). Ramsay (1980), Hilgers and Urai (2002), and Bons et al. (2012) argue that stretched veins are produced by numerous crack-seal events, and that the crystals in stretched veins typically have serrated boundaries or radiator structures owing to the opening in different positions of veins. In syntaxial veins, minerals grow from both sides to the centre of the veins. Thus, minerals fill space created by a cracking event (Wilson 1994; Bons et al., 2012). Antitaxial veins are characterized by a mineral growth from the centre toward both sides of the veins. The formation of antitaxial veins are still debated. Indeed, several key mechanisms seem to

69 be involved and widely studied as the natural hydraulic fracturing, the force of crystallisation,
70 the tectonic stresses, and the pression dissolution (Bons et al., 2012; Zanella, 2013).

71 Because of the special crystal morphology, the formation mechanism of antitaxial
72 veins have been extensively discussed in terms of formation and growth process (Durney and
73 Ramsay, 1973; Ramsay, 1980; Cox, 1987; Urai et al., 1991; Passchier and Trouw, 1996; Means
74 and li, 2001; Bons and Montenari, 2005; Rodrigues et al., 2009; Bons et al.,2012; Cobbold et
75 al., 2013; Meng et al., 2017a, 2017b, 2017c, 2018a; Luan et al., 2019; Zhao et al., 2020) and
76 Larmier et al. (2021) showed that BPV are complex and record many structural events during
77 their growth. The published data agreed that the hydraulic fracture caused by fluid
78 overpressure is most likely the cause of the BPV formation (Sherman et al., 1972; Stoneley et
79 al., 1983; Cosgrove t al., 2001; Philipp, 2008; Rodrigues et al., 2009; Li et al., 2013; Cobbold et
80 al., 2013; Zanella et al., 2014, 2015a, 2015b; Meng et al., 2017a, 2017b; Wang et al., 2018).
81 Several key parameters are furthermore involved in the formation of the BPV such as the fluid
82 overpressure (e.g. Mourgues & Cobbold, 2003; Cobbold & Rodrigues, 2007; Zanella et al.,
83 2014, 2015a, 2015b; Meng et al., 2017a, 2017b; Wang et al., 2018), the generation of
84 hydrocarbons (Zanella et al., 2014, 2015a, 2015b), the force of crystallization (Keulen et al.,
85 2001; Means and Li, 2001; Barker et al., 2006; Nollet et al., 2009; Bons et al. 2012; Wang et
86 al., 2018; Meng et al., 2018b, 2019) and the tectonic stresses (Meng et al., 2017b; Ukar et al.,
87 2020; Zanella et al., 2020).

88 Gypsum BPV have been extensively studied and often associated with hydraulic
89 fracturing process (Shearman et al., 1972; Machel, 1985; Gustavson et al., 1994; El Tabakh et
90 al., 1998; Cosgrove, 2001; Ahmadi, 2006; Philipp, 2008; Cobbold et al., 2013; Rustichelli et al.,
91 2016; Meng et al., 2017b, 2017c, 2019; De Toffoli et al., 2020; Zhao et al., 2020). Thus,
92 anhydrite hydration to gypsum with volume increase and injection of external fluid are

93 considered as the origin of fluid overpressure which leads to the formation of these BPV
94 (Philipp, 2008). However, Machel (1985) argued that the hydration of anhydrite is not
95 perquisite for the formation of fibrous gypsum veins, which may result from overpressure or
96 tectonic compression, or a combination of both processes. Meng et al. (2017b) and Berthelon
97 et al. (2021) have recently demonstrated that the occurrence of fluid overpressure can be a
98 consequence of tectonic compression during basin inversion. Osborne et Swarbrick (1997)
99 and Cosgrove (2001) also supported this point and argued that fluid overpressure may be
100 sufficiently high to form horizontal BPV during basin inversion. In addition, halite dissolution
101 and sediments exhumation were also proposed to be the origin of gypsum BPV (Gustavson et
102 al., 1994; El Tabakh et al., 1998). In a recent review, Zanella et al. (2020) demonstrated that a
103 compressive tectonic activity is required to generate BPV and highlighted the importance of
104 the force of crystallization during such geological processes.

105 The study of the BPV, especially gypsum BPV, is not well developed in the northern
106 part of Africa. There is a dearth of published data about these BPV structures (Ahmadi, 2006;
107 Akrout et al., 2011a). In the Ghdames Basin, southern Tunisia, a significant overpressure
108 interval was highlighted and well characterized by Akrout (2012) and gypsum BPV are
109 identified in the Liassic sediments especially in the Zmilet Haber Fm.

110 In this contribution, we combine structural and petrographic analysis on gypsum BPV,
111 host mudstones and evaporites from the Bouhedma Formation exposed in the ZBAS (Zemlet
112 El Beidha Anticline Structures), Southern Tunisian Atlas (Fig. 1) in order to investigate
113 distribution and timing of generation of such BPV.

114

115

2. Geological setting

2.1. Tectonic setting

The tectonic evolution of the African and Eurasian plates during the Meso-Cenozoic Era has appeared with the creation of distinct structural domains with several fault and anticlines (Philip, 1987; Chihi and Philip, 1999; Bouaziz et al., 2002) (Fig. 1A). From north to south, three domains are identified in Tunisia, Northern part of the African plate (Fig. 1A): the Tellian domain, the fold Atlasic domain (including the Northern Tunisian Atlas, The Middle Tunisian Atlas and the Southern Tunisian Atlas) and the Saharian platform (Fig. 1A). In the south, the southern Tunisian Atlas fold-and-thrust belt (Fig. 1A) is limited by two major NW trending faults systems: the Gafsa fault system and the Negrine-Tozeur fault system (Zargouni et al., 1985; Abbès and Zargouni, 1986; Burollet, 1991; Abbès et al., 1994; Zouari, 1995; Zouari; 1999; Hlaiem, 1998, 1999; Bédir, 2001; Gharbi et al., 2014) (Fig. 1). The Gafsa fault system (N140°) affects the Bou Ramli, the Ben Younes and the Orbata anticlines in the northern part and the Zemlet el Beidha (our area of study) and the Koudiat Hammamet anticlines in the southern part (Zargouni, 1984; Zargouni et al., 1985; Abbès and Zargouni, 1986; Burollet, 1991; Abbès et al., 1994; Boutib and Zargouni, 1998; Hlaiem,1999). The Negrine-Tozeur fault system, which borders the west of the Gafsa-Metlaoui basin, is parallel to the Gafsa fault system (Zargouni, 1984; Zargouni et al., 1985) (Fig. 1).

"Figure 1 here"

Our area of study, the Zemlet el Beidha Anticline Structure ZBAS, belongs to the southern Atlasic front of Tunisia in the eastern part of the E-W trending northern Chotts range, is oriented N060° to N030° (Figs. 1). Based on the previous tectonic study in Tunisia we identified two major tectonic phases which are responsible for the growth and deformation

139 of the majority of anticline due to compressive tectonic stresses occurring from the Neogene
140 to current times. A tectonic phases characterized by the NW - SW shortening direction is
141 attributed to the serravalian-Tortonian age, and another phases characterized by NNW-SSE to
142 N-S shortening direction is attributed to post-villafranchian age (Fig. 2). This area consists of a
143 south-verging asymmetrical anticline with a curved axis, which curves from E-W to NE-SW
144 orientation (Abdeljouad and Zargouni, 1981; Zargouni and Ruhland, 1981; Zargouni et al.,
145 1985; Gharbi et al., 2013). The southern forelimb of the ZBAS commonly displays subvertical
146 faults, previously interpreted by several authors as strike-slip faults (Abdeljouad and Zargouni,
147 1981; Zargouni et al., 1985; Abbes et al., 1994; Gharbi et al., 2013; Haji et al., 2020). The ZBAS
148 rests between the Southern Atlasic fold-and thrust belt to the north and the little deformed
149 Saharan Platform to the south (Zargouni, 1984; Ben Ferjani et al., 1990; Burollet, 1991;
150 Hlaiem, 1999; Bouaziz et al., 2002) (Fig. 1B). The ZBAS is affected by E-W fault trend
151 southward and by N-S fault trend northward (Louhaïchi and Tlig, 1993). Thus, in this area, the
152 Miocene and the Quaternary are considered as the major compressive phases in Atlasic areas
153 in Tunisia, in particular in the Chotts range (Fig. 2) (Ahmadi, 2006; Ouali, 2007; Ahmadi et al.,
154 2019; Khalfi et al., 2019).

155 “Figure 2 here”

156 ## 2.2. Sedimentary setting

157 Lithostratigraphic sequences in Tunisia’s southern Atlas are characterized by
158 significant lateral variations in thickness and facies based on outcrops data (Gharbi, 2013).
159 The Lower Cretaceous series contain a siliciclastic, clay, dolomites and sandstones layers.
160 From bottom to top, the following formations are described (Figs. 1C and 3): the Bouhedma
161 Fm. (400 to 2000 m thick carbonates-clays-evaporites sequence (Hauterivian), Abdeljouad

and Zargouni, 1981; Lazzez and Ben Youssef, 2008), The Sidi Aïch Fm. (200 m thick sequence of shaly sandstones and ferruginous sandstones (Barremian), Abbès and Tlig, 1991; Louhaïchi and Tlig, 1993; Ben Youssef and Peybernes, 1993; Chaabani and Razgallah, 2006; Gharbi, 2013; Boukhalfa 2015: Li et al., 2017), Orbata Fm. (dolomites, marls and sandstones (Aptian), Ben Youssef and Peybernes, 1993), Zebbag Fm. (marls, dolomites, evaporites (Albian-Turonian), Aleg Fm. (marls, limestones and evaporites (Turonian-Early Campanian). The Segui Fm, interpreted as syntectonic deposits acknowledged to be the product of erosion of the uplifted structures during Cenozoic compressional events, rest unconformably over the Neogene and Cretaceous Formations (Gharbi, 2013).

The sedimentary rocks crop out well in the ZBAS area, especially those of lower Cretaceous to late Miocene ages (Figs. 1C and 3). The lithostratigraphic chart of the Cretaceous series shows three principal formations, in ascending order (Figs. 3 and 4) (Abdeljouad and Zargouni, 1981; M'Rabet, 1981; Abbées and Zargouni, 1986; Gharbi et al., 2013; Boukhalfa et al., 2015): The Bouhedma Formation, was introduced by Burollet (1956) and M'Rabet (1981) at the locality type of Jebel Bouhedma in the south of Tunisia. In the ZBAS area, about 70 km to the south of the type locality, the Bouhedma Formation is described as a thick succession (120-900m) of limestones, dolomites, evaporites and sandstones (Abdeljouad and Zargouni, 1981; Gharbi et al., 2013; Boukhalfa et al., 2015). The exact age of the formation is still debated (Fig. 3C). M'Rabet (1981) assigned the Bouhedma Formation at the Gafsa Basin (Jebel Sidi Aïch) to the Barremian. Damotte et al., (1987) attributed the fossiliferous (ostracods and echinoids) claystones (equivalent lower part of the Bouhedma Formation at Jebel Mrhila, central Tunisia), to the upper Hauterivian, based on ostracods assemblage while Chakhma et al., (1990) proposed a Hauterivian–upper Barremian age based on the fossiliferous claystones (Fig.1C and 3).

186 “Figure 3 here”

187 The Bouhedma Formation is overlain by the shale-rich sands and ferruginous
188 sandstones of the Sidi Aich Formation. Being 70 m thick, this formation was introduced by
189 Burollet (1956) from the typical locality at Jebel Sidi Aich in southwestern Tunisia (Boukhalfa,
190 2015) (Fig. 1C and 3). The massive dolomites of the Orbata Formation (lower Aptian) overlain
191 the Sidi Aich (Ben Youssef and Peybernes, 1993; Chaabani and Razgallah, 2006; Gharbi et al.,
192 2013). The Upper Albian deposits are rarely exposed in the ZBAS. They are dominated by
193 dolomitic sandstones, marls, limestones and argillaceous limestones. The Coniacian-Santonian
194 series of the Aleg Formation unconformably overlie the previous series, by a thick sequence
195 of dolomitic sandstones at the base, green marls and bioclastic limestones (Abbès and Tlig,
196 1991; Louhaïchi and Tlig, 1993; Gharbi, 2013). The Abiod Formation conformably overlies the
197 Aleg Formation and consists of limestone banks with intercalations of thin clay layers
198 (Abdeljaouad and Zargouni, 1981; Louhaïchi and Tlig, 1993; Gharbi, 2013), (Fig. 3). The
199 Cenozoic series of the studied area are composed by thin Palaeocene marine marls covered
200 by Paleogene and Neogene continental sediments.

201 **3.** Method

202 In order to investigate the distribution and the timing of formation of the BPV in the
203 Bouhedma Formation (Southern Tunisia), we performed a structural analysis on the BPV and
204 host rocks from the Zemlet el Beidha Anticline Structure ZBAS with field work over about 8
205 weeks (Fig. 1C). All our data come from the ZBAS but we paid particular attention to the
206 ‘Khanguet Aicha’ cross-section located in the southern-eastern part of our area of study ([A-
207 A’] on Figs. 1C and 4). First, we established a sedimentological log from field observations
208 along the ‘Khanguet Aicha’ stratigraphic log to be able to study the BPV distribution in the

209 sedimentary sequence. Regarding the BPV, we have been focussing on their distribution, their
210 size (continuous or discontinuous), internal structures (fibre morphology) and spatial
211 orientation. Because of the complexity of the BPV shape, we established a continuity criterion
212 as following: “continuous” BPV refers to the BPV with a total length greater than 1 m and
213 “discontinuous” BPV refers to BPV with a total length up to 1 m. All data from the BPV
214 measurements are synthetized on Figure 4 and Table 1.

215 The petrographic observations of the BPV have been performed on 18 thin sections
216 coming from samples located in the ZBAS. All these observations have been made with a
217 ZEISS AXIO Zoom V16. For accurate analysis of the relationships between BPV formation and
218 other tectonic structures, we have measured faults and folds geometries as well as non-
219 fibrous gypsum-filled fractures, we have used the WINTENSOR and STERONET software for
220 the stereographic projection of the fracture orientations (Faults and BPV).

221 ## 4. Results

222 ### 4.1. BPV distribution

223 Gypsum BPV are widespread in the whole ZBAS area (Fig. 1C). Due to the greater
224 exposure of the Bouhedma Fm. along the southern limb of the anticline, we observed more
225 BPV in this area compare to northern limb of the anticline. BPV exclusively occurred within
226 the Bouhedma Fm. from the base to the middle part (Fig. 4). They are not equally distributed
227 throughout the sedimentary sequence and are often concentrated around gypsum-bearing
228 layers, which concentrate 35% of the total amount of BPV levels (Figs.4 and 5). We also
229 observed that the BPV occur close to major tectonic discontinuities such as faults and
230 fractures (Fig. 4). No occurrence of the BPV has been observed in other sedimentary
231 formations.

232 “Figure 4 here”

233 “Table 1 here”

234 The BPV are mainly parallel to the bedding but some of them seem to be more oblique
235 in particular those that are discontinuous (Figs. 5A, 5B and 6). Continuous BPV are more
236 present at the sedimentary interfaces. Indeed, the interface between mudstones and gypsum
237 layers is often marked by a BPV occurrence (Fig. 5B and D). Within gypsum layers, very thin
238 layers of mudstones are also marked by continuous BPV occurrences (Fig. 5F), which may also
239 occur within mudstones layers. In this case, they are mainly localized at the center of the
240 layer. Discontinuous BPV especially occur within strata of gypsum (Fig. 5C, 5E and 5F). They
241 consist of a stack of many BPV levels which is very dense, a few millimeters separating the
242 different BPV strands. In some cases, it is difficult to separate each of them (Fig. 5C and 5F).
243 As consequence, we noted this occurrence as one strand of BPV.

244 “Figure 5 here”

245 The thickness range for the BPV population is large, the continuous BPV thickness
246 varied from 2 cm up to 18 cm (e.g. sample KA39, Fig. 5D and 5C), while the discontinuous BPV
247 show a thickness range between 1 mm and 5 cm (Table 1).

248 ## 4.2. BPV Morphology

249 BPV are mostly parallel to the bedding in the Bouhedma Formation. This is also the
250 case for the discontinuous BPV organized in several veins layers. ‘En-echelon’ structures are
251 common in such examples and the BPV seem to be all connected (Figs. 6 and 7). Some of the
252 lenticular fragments of the host rock can be embedded and integrated in the echelon veins,
253 creating oblique bridge frameworks towards the vein walls (Fig. 6C and 6C’). ‘En-echelon’

structures seem to connect two or more BPV levels (Fig. 7B&D). There are especially present at facies boundaries and close to folds. Most of the BPV exhibit the 'typical' internal morphology. Thus, the BPV show a median line from which the minerals started to growth toward the edges of the veins (Figs. 6A and 7C). The median line is located usually at the middle of the vein but could be near the edges. The median line in marked by small fragments of mudstones (Fig.8C and C'). In many cases, we did not observe a median line within BPV (Fig. 6B and 6B'). In those BPV, gypsum fibers span the entire of the veins (Fig. 6B and 6B').

"Figure 6 here"

Several BPV display a sigmoidal morphology and the fibers are, consequently, not always perpendicular to the edges of the veins (Figs. 6, 7 and 10 C). The gypsum fibers, irrespective of their location and curvatures, are all oriented 135° - 165° (trend line) (Fig.9). In some cases, fibers are perpendicular to the median line at the middle of the vein and become parallel toward the edges (Fig. 7F and 7G). For example, between sub vertical fibers and gypsum veins walls of steep veins, an angle of 58° is indicating in figure 7E. Vein sizes vary from 2 to 18 cm in thickness, and 5 cm to over tens meters in length in the Khanguet Aicha section (Figs.4 and 5).

"Figure 7 here"

In the ZBAS, a high number of oblique gypsum veins are detected, especially near the BPV (Figs. 6D, 7A and 7B). Adjacent BPV are usually connected by oblique veins, with apparent interconnection and interaction (Fig. 7A and 7B). In some cases, there is relatively closed spacing between adjacent veins (Figs. 5A , 5B and 7D). Furthermore, numerous gypsum veins are mutually crosscutting and appear in a dense network without obvious overprinting relationships (Figs. 5F, 6 and 7), suggesting that these veins were probably

277 formed simultaneously as already show by Zhao et al. (2020). Such characteristics of gypsum
278 veins were also described by Philipp (2008) in the Bristol Channel Basin (Somerset, SW
279 England). In such veins, the gypsum fibers are all oriented in the same direction regardless of
280 their localities and veins wall curvature (Figs. 6, 7 and 8).

281 At the end of the veins, branching is commonly observed (Fig.6C and 6C'). The total
282 thickness of branching veins (sum of them) is approximately equal to the parent vein (Meng
283 et al., 2017b).

284 ### 4.3. Petrography

285 The BPV of the Bouhedma Formation are mainly composed of fibrous gypsum (Fig. 8).
286 We also observed crystals of anhydrite especially in veins located close to gypsum layers (Fig.
287 8C and 8C'). Minerals seem to have grown continuously from the median line toward the
288 edges (Fig. 8D and 8D'). In some cases, several stages of growth can be noted (Fig. 8A, A' and
289 8B, B') the median line, by various wall rock fragments (Fig. 8C and 8C'), related to crack-
290 sealing process. The median section, however, consists sometimes of single line without
291 crystals being filled (Fig. 8A and 8C).

292 "Figure 8 here"

293 ### 4.4. Folds, faults and filled fractures

294 In the ZBAS area, tectonic activity has been recorded, since the Cenozoic times. We
295 identified many structures, such as folds and faults, related to these tectonic activities on the
296 filed (Figs. 9, 10 and 11). The analysis of the bedding planes shows that the major folded
297 structure affecting the ZBAS is an anticline fold (Fig. 9A). The anticline axis is oriented N 30°.
298 The dip of strata is higher in the southern limb (35-70° S) than the northern (4-12° N) limb

299 showing an asymmetry of the fold geometry with a curved axis that changes from an E to NE
300 trend from W to E (Fig.1). Thus, the hinge plane of the fold dip northward and the fold are
301 characterized with an inclined horizontal morphology. The axis of the fold slightly plunges
302 toward the Southwest.

303 "Figure 9 here"

304 Many faults occur in the ZBAS (Fig. 9, 10 and 11). Numerous faults have affected the
305 whole sedimentary sequence at different scale from centimeters to multi-kilometers scale
306 (Fig. 1C and 11). Our measurements show two main groups of faults (Fig. 9). The first is
307 oriented 100° - 110° and consists mainly of reversed faults affecting the folds. Fore thrusts
308 and back thrusts compose this group of faults (Fig. 11). They affect the sedimentary rocks as
309 well as the BPV and other filled fractures. The second group of faults is characterized by a
310 range of orientations from N130° to N175°. Because they represent weakness zones and thus
311 encourage local erosion, these faults are related to the formation of several wadis as the
312 Khanget AÏcha, Amor, Telmam or Dhaou (Fig. 3). This fault group is mainly composed of left-
313 lateral strike-slip faults, mostly sub-vertical.

314 "Figure 10 here"

315 We observed a large amount of oblique veins in the ZBAS. These fractures are mainly
316 oriented N125°-N170° (Fig.9) and do not cross-cut the whole Bouhedma Formation. They are
317 concentrated from the lower to the middle part of the sedimentary formation and seem to
318 preferentially affect mudstones and marls of the Bouhedma Fm (Figs. 4 and 11D). The
319 morphology of filled fractures are from decimeters to pluri decameters by length and from 1
320 to almost 30 cm in width (Table 1). Both gypsum and anhydrite crystals compose the fractures
321 (Fig. 8C and 8C'). Regarding the crystals shape, we observed several examples of fibrous

minerals as well as non-fibrous. Nevertheless, we didn't observe both fibrous and non-fibrous crystals in a same vein. In outcrop we identified that the biggest oblique filled fractures are composed by non-fibrous gypsum crystals. The relationship between the fibrous criterion and the localization of the fractures is still unclear.

4.5. Relationship between folds, faults, BPV and filled fractures

From our observations and measurements, we managed to get some information about the relationship between tectonic structures (folds, faults) and fluid assisted fractures (filled fractures and BPV). Regarding the folding, it affects the sedimentary rocks as well as the BPV. Curved fibers composing the BPV are good indicators to demonstrate the growth of the mineral during the deformation. The formation of both 'Z'(Fig. 11D). and 'S' (Fig. 11B). curved fibers along a single folded structure indicates the synchronicity between the folding and the BPV fibers growth (Fig. 11). Nevertheless, some of these the BPV don't have curved fibers. We observed many examples of reversed faults cross-cutting BPV as well as 'en-échelon' and duplex structures in BPV (Figs. 10 and 11) with clear thickness variations for BPV.

"Figure 11 here"

The relationship between oblique filled fractures and the BPV is partially understood. In fact, we observed three different interactions: i) the oblique fractures cross-cut the BPV, ii) both filled fractures and BPV are connected and iii) BPV cross-cut oblique veins (Figs. 8 and 11). Oblique filled fractures cross-cut folded sedimentary rocks and the folding seems to not affect their morphology.

5. Discussions

343 Bedding-parallel veins are very common in sedimentary basins worldwide. Many
344 previous studies have demonstrated the great interest of the understanding of such
345 geological features to upgrade our knowledge on the fluid-rocks interactions and potential
346 allied resources (e.g. Cobbold et al. 2013; Gale et al. 2014; Ukar et al. 2020; Zanella et al.
347 2020). Nevertheless, in Tunisia and especially in the Zemlet El Beidha Anticline Structure
348 (ZBAS), published works report BPV occurrences (Ahmadi, 2006; Akrout et al., 2011). In our
349 detailed study, we demonstrate that the BPV are frequently observed in the ZBAS area and
350 more specifically within the lower Cretaceous strata of the Bouhedma Formation (Fig.1C).
351 They especially occur from the lower to the middle part of the Formation and exhibit gypsum
352 and anhydrite fibrous crystals (Figs. 4, 5 and 8C'). The composition of BPV is a key parameter
353 to understand the origin of the fluid responsible of their formation. In this context, previous
354 studies demonstrated the role of the generation of fluid by chemical reactions such as the
355 generation of hydrocarbons (Rodrigues et al. 2009; Cobbold et al. 2013; Zanella et al. 2015a,
356 2015b) or mineralogical transformations (Sherman et al., 1972; Machel, 1985; Gustavson et
357 al., 1994; El Tabakh et al., 1998; Philipp, 2008). In the area of study, no potential source rock
358 for petroleum is present. The sedimentary rocks composing the Bouhedma Formation is
359 essentially made of a layering of mudstones, marls and gypsum strata with some occurrences
360 of sandstones in the upper part of the sequence. Due to this sedimentological composition,
361 we infer that both fluid production and fluid overpressure were driven by the mineralogical
362 transformations between anhydrite and gypsum. This idea is in accordance with numerous
363 previous studies focused on gypsum veins (Shearman et al., 1972; Machel, 1985; Gustavson
364 et al., 1994; El Tabakh et al., 1998; Cosgrove, 2001; Ahmadi, 2006; Philipp, 2008; Akrout et al.,
365 2011a; Cobbold et al., 2013; Rustichelli et al., 2016; Adouani et al., 2019; B De Toffoli et al.,
366 2020). In such a context, reactions between gypsum and anhydrite can occur due to the burial

of the basin and then during deformation and exhumation of sediments. Due to the very low permeability of gypsum, marls and mudstones, the fluid contained within the strata is trapped and thus localized within or at boundaries of gypsum levels (Fig.4). According to Larmier et al. (2021), the composition and internal structures of the BPV are much complex than previously described in the literature (Fig. 8). Indeed, the more continuous and thicker BPV are located very close to gypsum beds (Figs. 4 and 5). As consequence and due to its sandy composition, no BPV are noted in the upper part of the Bouhedma Formation. The localization of the BPV at boundaries of gypsum beds can also be explained by a mechanical characteristic. In fact, the boundaries between gypsum layers and other beds, such as marls and mudstones, constitutes a mechanical discontinuity acting like a weak plane which can be a preferential zone of fluid pathway and/or damage (Fig.4A and 4B). This particular transition of rheology can be activated due to fluid overpressures related to anhydrite/gypsum reactions. Ravier et al. (2020) and Larmier et al. (2021) demonstrated the role of such mechanical discontinuities in the localization of BPV. These mechanical behaviors and in this case the generation of weak planes, find its origins in the orbital parameters that drive the sedimentation (Ravier et al. 2020). One of our observations demonstrates the role of these discontinuities on the localization of the BPV. In this study, we indicate that continuous BPV are more present than discontinuous BPV at these discontinuities (Fig.4A and 4B). This selective difference may be attributed to the higher permeability of the discontinuities compare to both sedimentological edges. In consequence, overpressured fluids are concentrated in these particular levels and are likely to migrate laterally and open filled fractures then forming more continuous veins.

The presence of much amount of oblique and sub-vertical filled fractures at different scale in the ZBAS area complexifies the previous schematic representation of fluid migration within the Bouhedma Formation (Figs. 10 and 11). Our observations confirm that the

391 discernibility of these BPV depends on the presence of these filled fractures (Fig. 4). Even the
392 relationship between both oblique filled fractures and the BPV still misunderstood, we explain
393 this by the role of oblique veins on the migration of fluid through the sedimentary strata.
394 Thus, we suggest that both a part of the amount of the BPV and oblique filled fractures were
395 developed synchronously. (Fig.5 and Fig.6C & 6D) This is well demonstrated by the
396 connectivity between both features on Figure 11D.

397 The literature and our measurements demonstrate that the presence of filled
398 fractures, reverse faults and folds are the consequence of the shortening of the basin during
399 the Cenozoic (Zargouni, 1984; Ben Ferjani et al., 1990; Burollet, 1991; Chihi, 1992; Louhaïchi
400 and Tlig, 1993; Hlaiem, 1999; Bouaziz et al., 2002; Ahmadi, 2006; Ouali, 2007; Gharbi, 2013;
401 Gharbi et al., 2013; Ahmadi et al., 2019; Khalfi et al., 2019, Haji et al., 2020; Abdelkader et al.,
402 2020) (Fig. 2). The orientations of the major fold axis (N30°), reverse faults (N120°-N175) and
403 filled sub-vertical fractures (N100°-N110°) argue in favor of two main deformation periods
404 (Fig.9). We attach the first tectonic event to the major compressive event of the Miocene.
405 Indeed, numerous of our observations argue in favor of the development of the BPV during a
406 compressive period (Figs. 10 and 11). This is in particular well illustrated with the BPV curved
407 fibers (e.g. Fig. 10). Nevertheless, many faults cross-cut the BPV explained by the generation
408 of faults and oblique structures during the second major compressive event during the post-
409 Villafranchian times (Fig. 10 and Fig.11). Thus, we infer that the BPV development took place
410 from the Miocene until the post-Villafranchian times.

411 Regarding the formation of the BPV in the ZBAS, we think that the BPV are only
412 present in the Bouhedma Formation because of its composition and the frequent presence of
413 gypsum beds. We identify from our observations 3 mains periods of formation for the BPV.

414 Due to burial, chemical reactions affected the gypsum and reverse reaction of
415 dehydratation/hydratation of the gypsum leading to fluid overpressures and then natural fluid
416 assisted fracturing. As consequence, the first generation of localized, continuous and
417 discontinuous BPV occurred. This generation of BPV exhibits orthogonal and undeformed
418 fibers of gypsum. Then during the major tectonic compressive event, the overpressure rises
419 up and is generalized in the area creating new BPV, much continuous, as well as folds, faults
420 and some filled fractures. This generation of BPV shows curved fibers. Finally, during post-
421 Villafranchian times, other BPV, faults and filled oblique fractures are generated cross-cutting
422 the previous ones (Fig. 12).

423 Regarding the formation of Gypsum BPV in the Bouhedma Fm, there are two main
424 phases during the formation: (1) the initiation of the fracture, corresponding to the median
425 zone and (2) the filling of the fracture. As previously evocated in the literature, the initiation
426 of the fracture is related to several mechanisms as the fluid overpressure or the tectonic
427 stresses (Zhao et al. 2020; Zanella et al., 2021;). Regarding the filling of the BPV, previous
428 authors involved the mechanisms of the fluid overpressure, the force of crystallization and
429 the tectonic stresses. (Philipp, 2008 ; Ukar et al., 2017 ; Meng et al., 2018 ; Luan et al., 2019 ;
430 Meng et al., 2019 ; Zhao et al., 2020).

431 "Figure 12 here"

432 ## Conclusions

433 In this study, we demonstrate that bedding-parallel veins, BPV, are abundant and clearly
434 observed in the Bouhedma Formation, ZBAS (Northern Chotts range - Southern Tunisia). BPV
435 are not randomly distributed through the sedimentary rocks. They especially occur within the
436 lower part of the Formation and are mainly localized at boundaries between evaporitic beds

437 and mudstones. BPV affect the whole ZBAS demonstrating the high continuity of the BPV
438 propagation. Thus, we infer that sedimentary discontinuities play a major role on the
439 formation of weakness plans that facilitate the formation and propagation of fluid-assisted
440 fractures. Gypsum and anhydrite compose the BPV. Gypsum is dominant in term of
441 occurrence but both, gypsum and anhydrite, exhibit fibrous minerals. We think that BPV
442 origin is linked with mineralogical transformations between gypsum and anhydrite during
443 burial and then exhumation of the Bouhedma Formation. Indeed, the BPV fibers are often
444 highly deformed and show sigmoid and 'en-echelon' structures, indicating a deformation
445 during the fiber growth. These transformations led to fluid overpressure in the very low
446 permeable rocks which has been reinforced by the shortening of the basin. As consequence,
447 we suggest that BPV are mainly formed by a combination of several mechanisms as the
448 natural hydraulic fracturing and tectonic stresses of the Bouhedma Formation. Based on our
449 measurements, we demonstrate that BPV were developed in several stages from Miocene to
450 Villafranchian times.

451 ## Acknowledgments

452 The authors would like to thank, RIADH AHMADI (ENIS, Sfax, Tunisia) for his time and fruitful
453 scientific discussions as well as ABDELBACET TOUNEKTI, Faculty of Sciences of Tunis, for his
454 help on field work.

455 ## Figure caption

456 **Figure.1: (A)** Simplified structural sketch of west Mediterranean region with the location of
457 the Southern Atlas Front of Tunisia (modified from Masrouhi et al.,2019). **(B)** Schematic Lower
458 Cretaceous stratigraphy of Tunisia from a southern, landward, position toward the marine
459 north, **(C)** Geological map of the ZBAS (Louhaïchi and Tlig, 1993; Gharbi et al., 2013, Boukhalfa

et al., 2015) showing the Cretaceous outcrops and particularly the location of the Barremian biota site discovered in the Khanguet Aicha locality.

Figure. 2: Rose diagram synthesis of the compressive stress phases. Miocene and Quaternary are considered as the major compressive phases in Central Tunisia and Gafsa basin (modified from Ahmadi, 2006; Ouali, 2007; Ahmadi et al., 2019; Khalfi et al., 2019).

Figure. 3: The lithostratigraphical chart shows that the Bouhedma Formation is intercalated between two main lower Cretaceous detrital deposits of the Continental Intercalaire.

Figure. 4: Photographs of the BPV distribution in the Bouhedma formation **(A)** Continuous bedding-parallel veins in the Bouhedma Formation. **(B)** Discontinuous veins within gypsum layers. **(C)** Very dense network of the BPV in gypsum layers. **(D)** Example of continuous BPV developed within mudstones. G1: first generation & G2: second generation. The red lines mark the boundaries between both generations. **(E)** Continuous BPV in gypsum layer. **(F)** Dense gypsum fibres veins network.

Figure. 5: Detailed lithostratigraphic column of the Khanguet Aicha cross-section with lithological description and the BPV distribution along the Bouhedma Formation. The sampled BPV are highlighted by underlining a BPV numbers (from KA01 to KA46).

Figure. 6: Photographs showing the common morphologies of gypsum BPV and oblique veins in the Bouhedma Formation, ZBAS. **(A).** The BPV (12 cm thick) lining the central part of a mudstones sequence in Oued Khanguet Amor. **(B)** and **(B').** Continuous BPV (about 7 cm thick) within mudstones located in Oued Khanguet Aicha. **(C)** and **(C').** Complex of discontinuous BPV localized in a level of mudstones in Oued Khanguet Amor. **(D).** Oblique gypsum veins and BPV relationship in Oued Khanguet Dhaou.

Figure. 7: Photographs showing the common morphologies of gypsum BPV and oblique veins in the Bouhedma Formation, ZBAS. (A) and (B) Oblique veins developed between two BPV. (C) Oblique fibers in a sub-horizontal gypsum veins. (D) Oblique fibres in a BPV (KA29). (E) Oblique fibres in a sub-horizontal gypsum veins (KA14). (F and G) curved shape of the BPV indicating a shear component.

Figure. 8: Petrographic characteristics of the BPV. The gypsum veins are symmetrical about the median line. (A and A') According to textures and orientations of gypsum fibres, the BPV can be subdivided into 4 zone with the inclusion of the host rock. (B and B') According to textures and orientations of gypsum fibres, the BPV can be subdivided into 3 zone the orientation of the gypsum fibres as resulting from a shear component. (C and C') Curved gypsum crystals showing optical continuity. (D and D') Median zone without crystals filled and the arrows indicate direction of gypsum fibres growth. (E and E') BPV without median line.

Figure. 9: Stereographic projection of the fracture measurements (A) representation of the traces of the anticline's axis. (B) representation of faults affecting the studied area. (C) representation of BPV plans and fiber orientation.

Figure.10: Evidence for shortening in BPV. (A and B) the BPV contains single thrust fault, fault offsets inner zones, containing vertical fibers but not outer zone containing oblique fibers. (C and D) Bedding parallel veins tend to be slightly en echelon (GPS: X: 34.04392, Y: 9.78606), with sigmoidal tips provide evidence for linkage (GPS: 34.022231, 9.485914).

Figure. 11: (A) Anticline structure showing the relationship between BPV opening, deformation and sigmoidal and en echelon structure formation. (B and C) the BPV contains single thrust fault in the southern forelimb of the anticline structures. (D) BPV with a sigmoid

shape in the northern forelimb of the anticline structure indicating the shortening direction (E) BPV tend to be slightly en echelon, with sigmoidal tips provide evidence for linkage.

Figure. 12: Synthetic model of generation of BPV in the ZBAS area. 1. Initial stage of the Bouhedma Formation. 2. Burial before Miocene: generation of continuous and discontinuous BPV with orthogonal and undeformed fibers within or at boundaries of gypsum beds. 3. Shortening during Miocene: generation of BPV with curved fibers, 'en-échelon' structures, filled fractures, folds and faults. 4. Shortening during post-Villafranchian: generation of BPV with curved fibers and oblique filled fractures cross-cutting the first stage.

Table 1: Synthesis of the sampled BPV in the ZBAS.

References

Abbès, C., Zargouni, F., 1986. Anatomie d'un couloir de décrochements : le couloir de Hadifa (Chaîne Nord des Chotts-Tunisie). Rev. Sc. de la Terre, vol. 4, Tunisie.

Abbès, A., Tlig, S., 1991. Tectonique précoce et sédimentation de la série Crétacée dans le bassin des Chotts (Tunisie du sud). Géologie Méditerranéenne XVIII (3), 149–161.

Abbès, C., Abdeljaouad, S., Ben Ouezdou, H., 1994. Carte Géologique d'El Hamma au 1/100.000, feuille no. 74. Institut National de recherche Scientifique de Tunisie et Service Géologique Nationale d'Office Nationale de Mines, Tunisie.

Abdeljaouad, S., Zargouni, F., 1981. Mise en évidence d'une tectonique intracrétacé dans le secteur de J. Zemlet El Beïda (chaîne des Chotts). Acte de 1er Congr. Nat. Sc. Terre, Tunis, t. I, p. 285.

524 Abdelkader, S., Kadri, A., Ben Ayed, N., Kim, Y.S., Dooley, T. P., Rajabi, M., Braham, A.,
525 2020. Deformation styles related to intraplate strike-slip fault systems of the Saharan-
526 Tunisian Southern Atlas (North Africa): New kinematic models. Journal of Structural
527 Geology, 104175. https://doi.org/10.1016/j.jsg.2020.104175.

528 Adouani, S., Ahmadi, R., Khlifi, M., Akrout, D., Mercier, E., Montacer, M., 2019. Pore pressure
529 assessment from well data and overpressure mechanism: case study in Eastern Tunisia
530 basins. Mar Georesour Geotechnol. https://doi.org/10.1080/1064119X.2019.1633711

531 Ahmadi, R., 2006. Utilisation des marqueurs morphologiques, sédimentologique et
532 microstructuraux pour la validation des modèles cinématiques de plissement.
533 Application à l'Atlas méridional tunisien, Thèse de Doctorat, 215pp, Univ. Nantes,
534 Nantes. http://www.theses.fr/2006NANT2087

535 Ahmadi, R., Mercier, E., Trigui, H., Abdennaceur Ouali, J., 2019. Relationship between
536 fractures patterns and fold kinematics; the case study of Jebel Sehib, a typical fault
537 propagation fold of southern Tunisia. J. Afr. Earth Sci. 125, 23–35.
538 https://doi.org/10.1016/j.jafrearsci.2019.01.012

539 Akrout, D., Ahmadi, R., Mercier, E., Montacer, M., 2011a. Natural Hydrocarbon Accumulation
540 Related to Formation Overpressured Interval ; Study Case Is the Saharan Platform
541 (Southern Tunisia). Arabian Journal of Geosciences 5 (4): 849–857.
542 https://doi.org/10.1007/s12517-011-0287-6

543 Akrout, D., 2012. Caractérisation de la surpression de fluides interstitiels dans des forages
544 pétroliers : Essais de modélisation analogique et apport a l'étude des réservoirs et à

545 l'évolution structurale et organo-sédimentaire de bassin pétroliers du sud de la Tunisie.
546 Thèse Doct. Univ. De Sfax.

547 Barker, S.L.L., Cox, S.F., Eggins, S.M., Gagan, M.K., 2006. Microchemical evidence for episodic
548 growth of antitaxial veins during fracture-controlled fluid flow. Earth Planet. Sci. Lett.
549 250, 331–344. https://doi.org/10.1016/j.epsl.2006.07.051

550 Bédir, M., Boukadi, N., Tlig, S., Ben Timzal, F., Zitouni, L., Alouani, R., Slimane, F., Bobier, C.,
551 Zargouni, F., 2001. Subsurface Mesozoic basins in the central Atlas of Tunisia, tectonics,
552 sequence deposit distribution and hydrocarbon potential. AAPG Bull. 85 (5), 885–907.
553 https://doi.org/10.1306/8626CA2D-173B-11D7-8645000102C1865D

554 Ben Ferjani, A., Burollet, P., Mejri, F., 1990. Petroleum Geology of Tunisia. Entreprise
555 Tunisienne d'activités pétrolières(ETAP), Mémoire Ed, 194 p.
556 https://www.worldcat.org/title/petroleum-geology-of-tunisia/oclc/22480782

557 Ben Youssef, M., Peybernes, B., 1993. Données micropaléontologiques et biostratigraphiques
558 nouvelles sur le Crétacé inférieur marin du Sud tunisien. J. Afr. Earth Sci. 5, 217–231.
559 https://doi.org/10.1016/0899-5362(86)90013-8

560 Berthelon, J., Brüch, A., Colombo, D., Frey, J., Traby, R., Bouziat, A., Cacas-Stentz, M.C., Cornu
561 T., 2021. Impact of tectonic shortening on fluid overpressure in petroleum system
562 modelling: Insights from the Neuquén basin, Argentina. Mar. Pet. Geol. 127, 104933.
563 https://doi.org/10.1016/j.marpetgeo.2021.104933

564 Bons, P.D., Montenari, M., 2005. The formation of antitaxial calcite veins with well developed
565 fibres, Oppaminda Creek, South Australia. J. Struct. Geol. 27, 231–248.
566 https://doi.org/10.1016/j.jsg.2004.08.009

567 Bons, P.D., Elburg, M.A., Gomez-Rivas, E., 2012. A review of the formation of tectonic veins
568 and their microstructures. J. Struct. Geol. 43, 33–62.
569 https://doi.org/10.1016/j.jsg.2012.07.005

570 Bouaziz, S., Barrier, E., Soussi, M.M., Turki, M.M., Zouari, H., 2002. Tectonic evolution of the
571 northern African margin in Tunisia from paleostress data and sedimentary record.
572 Tectonophysics 357, 227–253. https://doi.org/10.1016/S0040-1951(02)00370-0

573 Boukhalfa, K., Li, G., Ben Ali, W., Soussi, M., 2015. Early Cretaceous spinicaudatans
574 ("conchostracans") from lacustrine strata of the Sidi Aïch Formation in the northern
575 Chotts range, southern Tunisia: Taxonomy, biostratigraphy and stratigraphic
576 implication. Cretaceous Research, 56, 482- 490.
577 http://dx.doi.org/10.1016/j.cretres.2015.06.006

578 Boutib, L., Zargouni, F., 1998. Disposition et géométrie des plis de l'Atlas centroméridional de
579 Tunisie. Découpage et cisaillement en lanières tectoniques. C. R. Acad. Sci. Paris 326,
580 261–265. https://doi.org/10.1016/S1251-8050(97)86816-4

581 Buckland, W., De la Beche, H.T., 1835. On the geology of the neighbourhood of Weymouth
582 and the adjacent parts of the coast of Dorset. Trans. Geol. Soc. Lond., s2 4, 1-46.

583 Burollet, P.F., 1956. Contribution à l'étude stratigraphique de la Tunisie centrale. Annales des
584 Mines et de la Géologie Tunisie, vol. 18, 350 p.

585 Chaabani, F., Razgallah, S., 2006. Aptian Sedimentation: An Example of Interaction between
586 Tectonics and Eustatics in Central Tunisia. Geological Society, London, Special
587 Publications, 262, pp. 55–74. http://dx.doi.org/10.1144/GSL.SP.2006.262.01.03

588 Chakhma, H., Donze, P., Razgallah, S., Memmi, L., 1990. Le Crétacé inférieur de la région de
589 Bir El Hafey, précisions chronostratigraphiques sur les formations Bouhedma, Sidi Aïch,
590 Orbata et Zebbag. Notes du Service Géologique de Tunisie 56, 9–18.

591 Chihi, L., Ben Haj Ali, M., Ben Ayed, N., 1992. Structural significance and mechanism of folding
592 in the Chott chain, southern Tunisia. Analogy with folds associated with the Sbiba strike-
593 slip fault, central Tunisia. C. R. Acad Sci II 315 (10), 1245–1252.

594 Cobbold, P.R., Rodrigues, N., 2007. Seepage forces, important factors in the formation of
595 horizontal hydraulic fractures and bedding-parallel fibrous veins ('beef' and 'cone-in-
596 cone'). Geofluids, v. 7, 313–322. https://doi.org/10.1111/j.1468-8123.2007.00183.x

597 Cobbold, P.R., Zanella, A., Rodrigues, N., Løseth, H., 2013. Bedding-parallel fibrous veins (beef
598 and cone-in-cone): worldwide occurrence and possible significance in terms of fluid
599 overpressure, hydrocarbon generation and mineralization. Mar. Petroleum Geol. 43, 1-
600 20. https://doi.org/10.1016/j.marpetgeo.2013.01.010

601 Cosgrove, J.W., 2001. Hydraulic fracturing during the formation and defor-mation of a basin:
602 A factor in the dewatering of low-permeability sedi-ments. Am Assoc Pet Geol Bull, 85,
603 737–748.

604 Cox, S.F., 1987. Antitaxial crack-seal vein microstructures and their relationship to
605 displacement paths. J. Struct. Geol. 9 (7), 779-787. https://doi.org/10.1016/0191-
606 8141(87)90079-4

607 De Toffoli, B., Mangold, N., Massironi, M., Zanella, A., Pozzobon, R., Le Mouélic, S.,
608 Cremonese, G., 2020. Analyse structurale des réseaux de veines de sulfate dans le

609 cratère Gale (Mars). Journal of Structural Geology, 104083. https://doi.org/10.1016 /
610 j.jsg.2020.104083

611 Damotte, R., Zghal, I., Bismuth, H., 1987. Les marnes de l'Hauterivien-Barrémien du Jebel
612 Mhrila (Tunisie centrale) : analyse biostratigraphique et contexte paléogéographique.
613 Cah. Micropaleontol. Nouv. Sér. 2 (2), 5-24.

614 Durney, D.W., Ramsay, J.G., 1973. Incremental strains measured by syntectonic crystal
615 growths. In: De Jong, K.A., Scholten, R. (Eds.), Gravity and Tectonics. Wiley, New York,
616 pp 67-96.

617 El Tabakh, M., Schreiber, B.C., Warren, J.K., 1998. Origin of fibrous gypsum in the Newark rift
618 basin, eastern North America: Journal of Sedimentary Research, v. 68, p. 88-99.
619 http://dx.doi.org/10.2110/jsr.68.88

620 Gale, J.F.W., Laubach, S.E., Olson, J.E., Eichhubl, P., Fall, A., 2014. Natural fractures in shale: a
621 review and new observations. AAPG Bull. 98 (11), 2165e2216.
622 http://dx.doi.org/10.1306/08121413151

623 Ghrabi, M., 2013. Relationship between the southern Atlas foreland and the eastern margin
624 of Tunisia (Chotts-Gulf of Gabes): Tectono-sedimentary, fault kinematics and balanced
625 cross section approaches. Ph D Thesis, Univ. of Sfax, Tunisia, 202 p.
626 http://www.theses.fr/2013AIXM4340/document

627 Gharbi, M., Masrouhi, A., Espurt, N., Bellier, O., El Amari, A., Ben Youssef, M., Ghanmi, M.,
628 2013. New tectono-sedimentary evidences for Aptian to Santonian extension of the
629 Cretaceous rifting in the northern Chotts range (southern Tunisia). J. Afr. Earth Sci.
630 79:58-73. http://dx.doi.org/10.1016/j.jafrearsci.2012.09.017

631 Gharbi, M., Bellier, O., Masrouhi, A., Espurt, N., 2014. Recent spatial and temporal changes in
632 the stress regime along the southern Tunisian Atlas front and the Gulf of Gabes: new
633 insights from fault kinematics analysis and seismic profiles. Tectonophysics 626, 120–
634 136. http://dx.doi.org/10.1016/j.tecto.2014.04.00

635 Gustavson, T.C., Hovorka, S.D., Dutton, A.R., 1994. Origin of satin spar veins in evaporite
636 basins. J. Sediment. Res. 64, 88–94. https://doi.org/10.1306/D4267D1B-2B26-11D7-
637 8648000102C1865D

638 Haji, T.A., Moumni, Y., Msaddek, M.H., 2020. Fault-style analysis and seismic interpretation:
639 implications for the structural issues of the South-eastern Atlas in Tunisia. J. Afr. Earth
640 Sci. 172, 103962. https://doi.org/10.1016/j.jafrearsci.2020.103962

641 Hezzi, I., 2014. Caractérisation géophysique de la plateforme de Sahel, Tunisie nord-orientale
642 et ses conséquences géodynamiques. Géophysique [physics.geo-ph]. Université Rennes
643 1. Français. tel-00995595v1.

644 Hilgers, C., and J. L. Urai, 2002b, Microstructural observations on natural syntectonic fibrous
645 veins: implications for the growth process: Tectonophysics, v. 352, p. 257-274.
646 https://doi.org/10.1016/S0040-1951(02)00185-3

647 Hlaeim, A., 1999. Halokinesis and structural evolution of the major features in Eastern and
648 Southern Tunisian Atlas. Tectonophysics 306, pp 79-95. https://doi.org/10.1016/S0040-
649 1951(99)00045-1

650 Hlaiem, A., 1998. Etudes géophysiques et géologiques des bassins et des chaines de Tunisie
651 centrale et méridionale durant le mésozoïque et le Cénozoïque. Thèse Doctorat, Univ.
652 Des Pierre & Marie Curie Paris 6.

653 Keulen, N.T., den Brok, S.W.J., Spiers, C.J., 2001. Force of crystallisation of gypsum during
654 hydration of synthetic anhydrite rock. In: 13th DRT Conference, Deformation
655 Mechanisms, Rheology, and Tectonics, Noordwijkerhout, The Netherlands.

656 Khalfi, C., Ahmadi, R., Trigui, H.,Ouali, J., Mercier, E., 2019. Kinematic Evolution Model of
657 Fault-Related Anticline based on the Study of the Striated Pebbles of the Related
658 Growth-Strata: A Case Study of the Es Satah Anticline in Southern Tunisian Atlas,
659 Tunisia. Geotecton. 53, 419-432. https://doi.org/10.1134/S001685211903004X

660 Larmier, S., Zanella, A., Lejay, A., Mourgues, R., and Gelin, F., 2021. Geological parameters
661 controlling the bedding-parallel vein distribution in Vaca Muerta Formation core data,
662 Neuquén Basin, Argentina. AAPG Bulletin, DOI:10.1306/03122119201

663 Lazzez, M., Zouaghi, T., Ben Youssef, M., 2008. Austrian phase on the northern African margin
664 inferred from sequence stratigraphy and sedimentary records in southern Tunisia
665 (Chotts and Djeffara areas). C.R. Geosci. 340(8), 543–555.
666 https://doi.org/10.1016/j.crte.2008.05.005

667 Li, W., Dong, Y., Guo, A., Liu, X., Zhou, D., 2013. Chronology and tectonic significance of
668 cenozoic faults in the liupanshan arcuate tectonic belt at the northeastern margin of the
669 qinghai–tibet plateau. J. Asian Earth Sci. 73, 103–113.
670 https://doi.org/10.1016/j.jseaes.2013.04.026

671 Li, G., Boukhalfa, K., Teng, X., Soussi, M., Ali, W.B., Ouaja, M., Houla. Y., 2017. New Early
672 Cretaceous clam shrimps (Spinicaudata) from uppermost Bouhedma Formation of
673 northern Chotts range, southern Tunisia: taxonomy, stratigraphy and

674 palaeoenvironmental implications Cretac. Res., 72 (2017), pp. 124-133.
675 https://doi.org/10.1016/j.cretres.2019.01.025

676 Louhaïchi, M.A., Tlig, S., 1993. Tectonique synsédimentaire des séries post Barrémiennes au
677 Nord-Est de la chaîne Nord des Chotts (Tunisie méridionale). Géologie Méditerranéenne
678 XX(1), 53–74.

679 Luan, G., Dong, C., Azmy, Karem, Lin, C., Ma, C., Ren, L., Zhu, Z., 2019. Origin of bedding-
680 parallel fibrous calcite veins in lacustrine black shale: a case study from Dongying
681 Depression, Bohai Bay Basin. Mar. Pet. Geol. 102, 873–885.
682 https://doi.org/10.1016/j.marpetgeo.2019.01.010

683 Machel, H. G., 1985, Fibrous gypsum and fibrous anhydrite in veins: Sedimentology, v. 32, p.
684 443- 454. https://doi.org/10.1111/j.1365-3091.1985.tb00523.x

685 Masrouhi, A., Gharbi, M., Bellier, O., Youssef, M.B., 2019. The Southern Atlas Front in Tunisia
686 and its foreland basin: structural style and regional-scale deformation. Tectonophysics
687 764, 1–24.

688 Means, W.D., Li T., 2001. A laboratory simulation of fibrous veins: some first observations. J.
689 Struct. Geol. 23, 857-863. https://doi.org/10.1016/S0191-8141(00)00158-9

690 Meng, Q., Hooker, J., Cartwright, J., 2017a. Early overpressuring in organic-rich shales during
691 burial: evidence from fibrous calcite veins in the Lower Jurassic Shales-with- Beef
692 Member in the Wessex Basin, UK. J. Geol. Soc. 174, 869–882.
693 http://dx.doi.org/10.1144/jgs2016-146

694 Meng, Q., Hooker, J., Cartwright, J., 2017b. Genesis of natural hydraulic fractures as an
695 indicator of basin inversion. J. Struct. Geol. 102, 1–20. Meng, Q., Hooker, J., Cartwright,

696 J., 2017c. Lithological control on fracture cementation in the Keuper marl (Triassic),
697 north Somerset, UK. Geol. Mag. 1–15. https://doi.org/10.1016/j.jsg.2017.07.001

698 Meng, Q., Hooker, J., Cartwright, J., 2017c. Lithological control on fracture cementation in the
699 Keuper marl (Triassic), north Somerset, UK. Geol. Mag. 1–15.
700 https://doi.org/10.1017/S001675681700070X

701 Meng, Q., Hooker, J., Cartwright, J., 2018a. Role of pressure solution in the formation of
702 bedding-parallel calcite veins in an immature shale (Cretaceous, southern UK). Geol.
703 Mag. 1–17. https://doi.org/10.1017/S0016756818000377

704 Meng, Q., Hooker, J., Cartwright, J., 2019. Progressive accretion of antitaxial crystal fibres:
705 implications for the kinematics and dynamics of vein dilation. J. Struct. Geol. 126, 25–
706 36. https://doi.org/10.1016/j.jsg.2019.05.006

707 Mourgues, R., Cobbold, P.R., 2003. Some tectonic consequences of fluid overpressures and
708 seepage 629 forces as demonstrated by sandbox modeling. Tectonophysics 376, 75-97.

709 M'Rabet, A., 1981. Stratigraphie, sédimentation et diagenèse carbonatée des séries du
710 Crétacé inférieur de Tunisie Centrale. Unpubl. PhD thesis, Paris-Orsey: 540 p.

711 Nollet, S., Koerner, T., Kramm, U., Hilgers, C., 2009. Precipitation of fracture fillings and
712 cements in 633 the Buntsandstein (NW Germany). Geofluids 9, 373-385.

713 Osborne, M. J., and R. E. Swarbrick, 1997. Mechanisms for generating overpressure in
714 sedimentary basins: a reevaluation: AAPG bulletin, v. 81, p. 1023-1041.

715

716 Ouali J., 2007. Structures en rampes tectoniques (Modèles et exemples). Thèse
717 complémentaires, Univ. De Tunis El Manar.

718 Passchier, C.W., Trouw, R.A.J., 1996. Microtectonics. Springer Verlag, Berlin. Passchier, C.W.,
719 Urai, J.L., 1988. Vorticity and strain analysis using Mohr diagrams. J. Struct. Geol. 10,
720 755–763.

721 Philipp, S.L., 2008. Geometry and formation of gypsum veins in mudstones at Watchet,
722 Somerset, SW England. Geol. Mag. 145, 831–844.
723 https://doi.org/10.1017/S0016756808005451

724 Philip H., Andrieux J., Dlala M., Chihi L., Ben Ayed N., 1986. Evolution tectonique mio-
725 plioquaternaire du fossé de Kasserine (Tunisie Centrale) : Implication sur l'évolution
726 géodynamique récente de la Tunisie. Bull. Sco. Géol. France, (8), II, p.55-568.

727 Ramsay, J.G., 1980. The crack-seal mechanism of rock deformation. Nature 284, 135-139.
728 https://doi.org/10.1038/284135a0

729 Ravier, E., Martinez, M., Pellenard, P., Zanella, A., Tupinier, L., 2020. The milankovitch
730 fingerprint on the distribution and thickness of bedding-parallel veins (beef) in source
731 rocks. Marine and Petroleum Geology, Elsevier, 122, pp.104643. DOI:
732 https://doi.org/10.1016/j.marpetgeo.2020.104643

733 Rodrigues, N., Cobbold, P.R., Løseth, H., Ruffet, G., 2009. Widespread bedding parallel veins of
734 fibrous calcite ("beef") in a mature source rock (Vaca Muerta Fm, Neuquen Basin,
735 Argentina): evidence for overpressure and horizontal compression. J. Geol. Soc. Lond.
736 166 (4), 695-709. https://doi.org/10.1144/0016-76492008-111

737 Rustichelli, A., Di Celma, C., Tondi, E., Baud, P., Vinciguerra, S., 2016. Fibrous gypsum veins as
738 diffuse features and within fault zones: the case study of the Pisco Basin (Ica desert,
739 southern Peru). J. Struct. Geol. 173, 405–418. https://doi.org/10.1144/jgs2015-084

740 Shearman, D.J., Mossop, G., Dunsmore, H., and Martin, M., 1972. Origin of gypsum veins by
741 hydraulic fracture. Transactions of the Institute of Mining and Metallurgy, V81, p. 149-
742 155.

743 Stoneley, R., 1983. Fibrous Calcite Veins, Overpressures, and Primary Oil Migration. *AAPG*
744 *Bulletin* 1983; 67 (9): 1427–1428. Doi: https://doi.org/10.1306/03B5BA47-16D1-11D7-
745 8645000102C1865D

746 Ukar, E., Baqués, V., Laubach, S. E., & Marrett, R. 2020. The nature and origins of decameter-
747 scale porosity in Ordovician carbonate rocks, Halahatang oilfield, Tarim Basin, China.
748 Journal of the Geological Society, jgs2019–156. https://doi.org/10.1144/jgs2019-156

749 Urai, J.L., Williams, P.F., van Roermund, H.L.M., 1991. Kinematics of crystal growth in
750 syntectonic fibrous veins. J. Struct. Geol. 13, 823-836. https://doi.org/10.1016/0191-
751 8141(91)90007-6

752 Wilson, C.J.L., 1994. Crystal growth during a single-stage opening event and its implications
753 for syntectonic veins. Journal of Structural Geology 16, 1283e1296.
754 https://doi.org/10.1016/0191-8141(94)90070-1

755 Wang, M., Chen, Y., Song, G., Steele-MacInnis, M., Liu, Q., Wang, X., Zhang, X., Zhao, Z., Liu,
756 W., Zhang, H., Zhou, Z., 2018. Formation of bedding-parallel, fibrous calcite veins in
757 laminated source rocks of the Eocene Dongying Depression: A growth model based on
758 petrographic observations: International Journal of Coal Geology, v. 200, p. 18-35.
759 https://doi.org/10.1016/j.coal.2018.10.004

760 Weger, R.J., Murray, S.T., McNeill, D.J., Swart, P.K., Eberli, G.P., Rodriguez Blanco, L., Tenaglia,
761 686 M., Rueda, L., 2018. Paleo thermometry and distribution of calcite beef in the Vaca
762 Muerta 687 Formation, Neuquén Basin, Argentina. AAPG Bulletin, (submitted).

763 Zanella, A., 2013. Surpression de fluides et fracturation de roches mères en différents
764 contextes tectoniques : modélisation analogique et exemples de terrain. Sciences de la
765 Terre. Université Rennes 1. Français. ⟨NNT : 2013REN1S139⟩. ⟨tel-00980281⟩.

766 Zanella, A., Cobbold, P.R., Rojas, L., 2014b. Beef veins and thrust detachments in Early
767 Cretaceous source rocks, foothills of Magallanes-Austral Basin, southern Chile and
768 Argentina: Structural evidence for fluid overpressure during hydrocarbon maturation:
769 Marine and Petroleum Geology, v. 55, p. 250-261.
770 https://doi.org/10.1016/j.marpetgeo.2013.10.006

771 Zanella, A., Cobbold, P.R., Ruffet, G., Leanza, H.A., 2015a. Geological evidence for fluid
772 overpressure, hydraulic fracturing and strong heating during maturation and migration
773 of hydrocarbons in Mesozoic rocks of the northern Neuquén Basin, Mendoza Province,
774 Argentina. J. S. Am. Earth Sci. 62, 229e242. https://doi.org/10.1016/j.jsames.2015.06.006

775 Zanella, A., Cobbold, P.R., Boassen, T., 2015b. Natural hydraulic fractures in the Wessex Basin,
776 SW England: widespread distribution, composition and history. Mar. Pet. Geol. 68,
777 438e448. https://doi.org/10.1016/j.marpetgeo.2015.09.005

778 Zanella, A., P.R. Cobbold, P.R., Rodrigues, N., Loseth, H., Jolivet, M., F. Gouttefangeas, F., and
779 Chew, D., 2020. Source rocks in foreland basins: a preferential context for the
780 development of natural hydraulic fractures., (in press; preliminary version published
781 online Ahead of Print 28 August 2020): AAPG Bulletin.
782 https://doi.org/10.1306/08122018162.

783 Zargouni, F., 1984. Style et chronologie des déformations des structures de l'Atlas tunisien
784 méridional. Évolution récente de l'accident Sud-atlasique. C.R. Acad Sci. Paris 299(Série
785 II, no. 2), 179–196.

786 Zargouni, F., Rabiaa, M.C., Abbes, C., 1985. Rôle des couloirs de cisaillement de Gafsa et de
787 Negrine-Tozeur dans la structuration du faisceau des plis des chotts, éléments de
788 l'accident sud-atlasique. CRASC.P, 301; 11, 831-883.

789 Zargouni, F., Ruhland, M., 1981. Style de déformations du quaternaire récent lié au
790 coulissement de la faille de Gafsa et chronologie des phases tectoniques de l'Atlas
791 méridionale de Tunisie. C.R. Acad. Sc. Paris 292, 913-915.

792 Zhao, B., Li, R., Wu, X., Qin, X., Zhao, D., Khaled, A., & Liu, F., 2020. Petrography and isotopic
793 geochemistry of bedding-parallel fibrous gypsum veins in the Neogene Qingshuiying
794 Formation of the Ningnan Basin, North China: Insights for growth model of antitaxial
795 fibrous veins. Journal of Structural Geology, 132.
796 https://doi.org/10.1016/j.jsg.2019.103973

797 Zouaghi, T., I. Ferhi, M. Bédir, M. B. Youssef, M. Gasmi, and Inoubli M. H., 2011. Analysis of
798 Cretaceous (Aptian) strata in central Tunisia, using 2D seismic data and well logs,
799 Journal of African Earth Sciences, 61(1), 38-61.
800 https://doi.org/10.1016/j.jafrearsci.2011.05.002

801 Zouari, H., 1995. Evolution géodynamique de l'Atlas centro - méridional de la Tunisie :
802 stratigraphie, analyses géométrique, cinématique et tectono -sédimentaire. Thèse de
803 Doctorat d'État Université de Tunis II.

804 Zouari, H., Turki, M. M., Delteil, J., Stephan, J.-F., 1999. Tectonique transtensive de la
805 paléomarge tunisienne au cours de l'Aptien-Campanien. Bull. Soc. Géol. France 170 (3),
806 295–301.

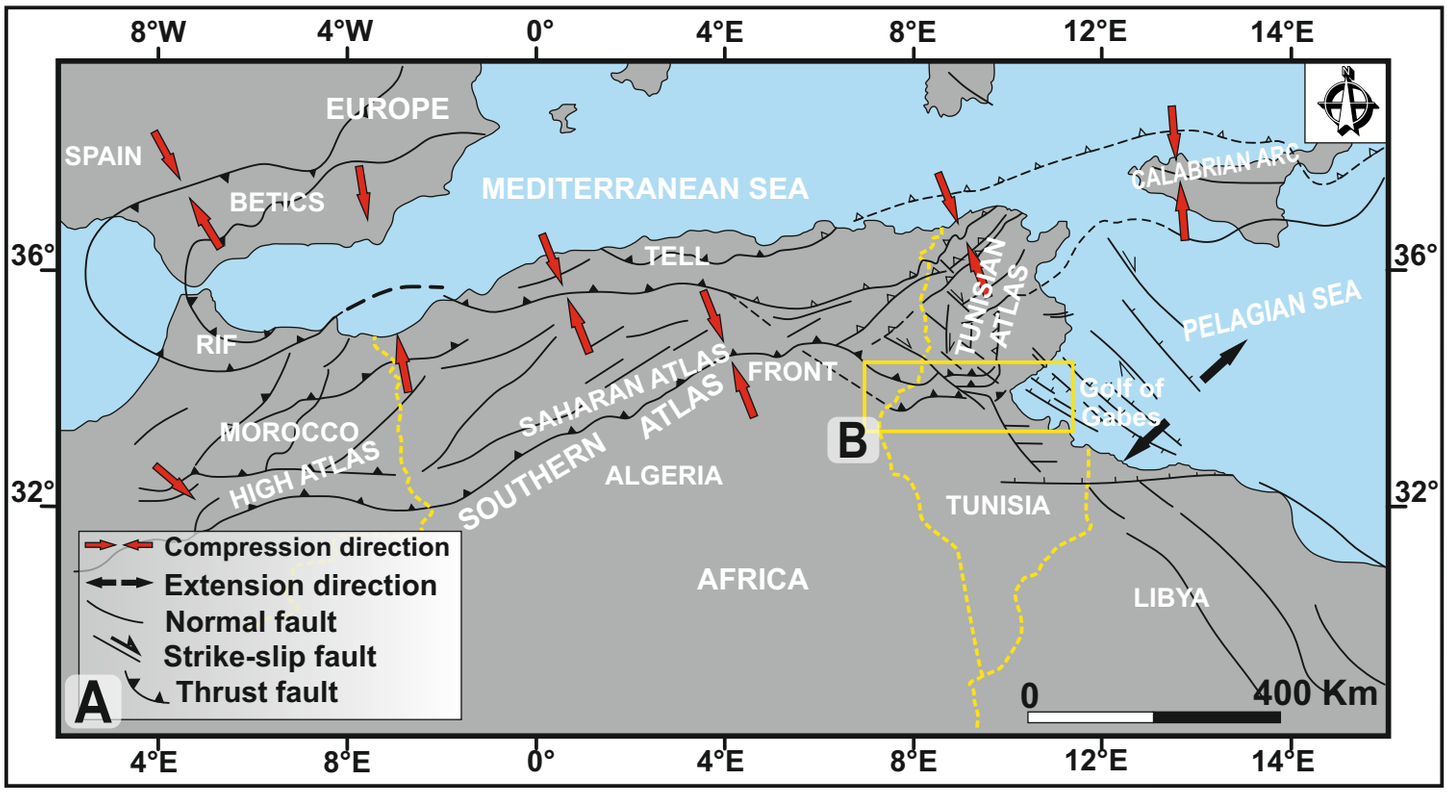
8°W
4°W
0°
4°E
8°E
12°E
14°E
36°
32°
EUROPE
SPAIN
BETICS
MEDITERRANEAN SEA
CALABRIAN ARC
TELL
TUNISIAN ATLAS
PELAGIAN SEA
RIF
SAHARAN ATLAS
FRONT
Gulf of Gabes
MOROCCO
HIGH ATLAS
SOUTHERN ATLAS
ALGERIA
B
TUNISIA
AFRICA
LIBYA
Compression direction
Extension direction
Normal fault
Strike-slip fault
Thrust fault
A
0
400 Km

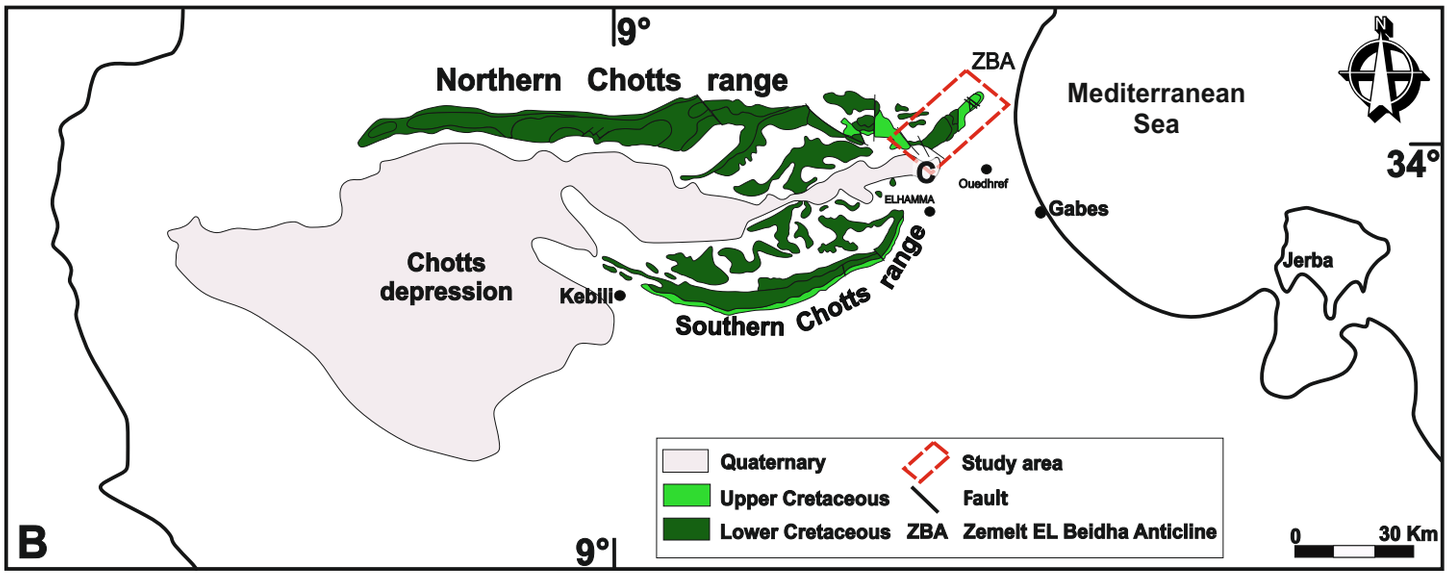
9°
Northern Chotts range
ZBA
Mediterranean Sea
N
34°
C
Ouedhref
ELHAMMA
Gabes
Chotts depression
Kebili
Southern Chotts range
Jerba
Quaternary
Upper Cretaceous
Lower Cretaceous
Study area
Fault
ZBA
Zemelt EL Beidha Anticline
B
0
30 Km

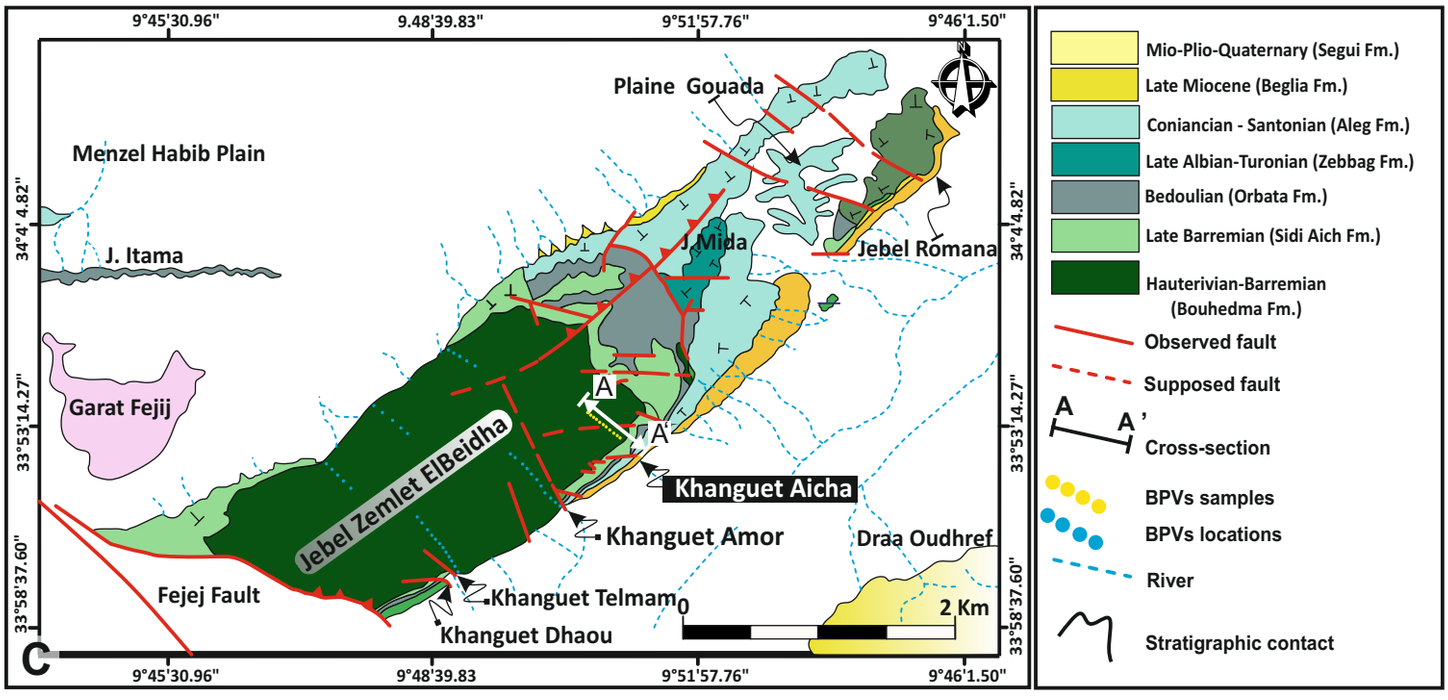
9°45'30.96"
9.48'39.83"
9°51'57.76"
9°46'1.50"
34°4'4.82"
33°53'14.27"
33°58'37.60"
Plaine Gouada
Menzel Habib Plain
J. Itama
J. Mida
Jebel Romana
Garat Fejij
A
A'
Jebel Zemlet ElBeidha
Khanguet Aicha
Khanguet Amor
Draa Oudhref
Fejej Fault
Khanguet Telmam
Khanguet Dhaou
0
2 Km
C
9°48'39.83
Mio-Plio-Quaternary (Segui Fm.)
Late Miocene (Beglia Fm.)
Coniancian - Santonian (Aleg Fm.)
Late Albian-Turonian (Zebbag Fm.)
Bedoulian (Orbata Fm.)
Late Barremian (Sidi Aich Fm.)
Hauterivian-Barremian (Bouhedma Fm.)
Observed fault
Supposed fault
A A'
Cross-section
BPVs samples
BPVs locations
River
Stratigraphic contact

Compressive events

1. Minor phases: Eocene

Addoumi (1995)	N120-150
Bracène et Frizon (2002)	N140-150
Le Ghali et al., (2003)	N170-180
Frizon et al., (2000)	N140-150
Pariat et al., (2003)	N160-170
Vially et al., (1994)	N120-130
Yaïch (1984)	N130
Zouari (1995)	N175
Zargouni (1986)	N140

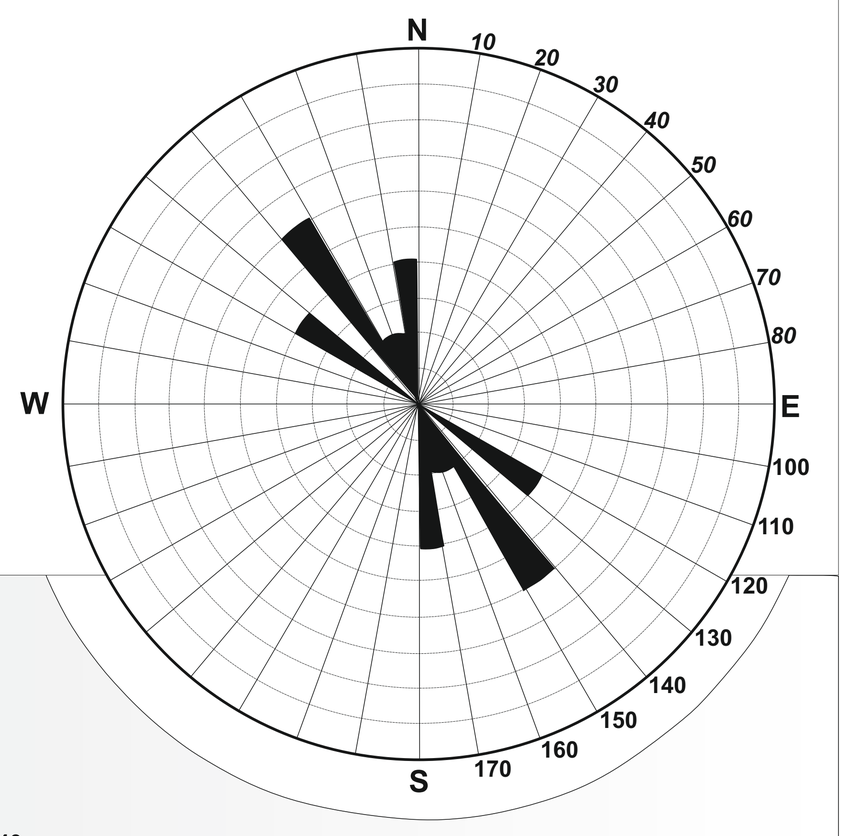

2. Major phases: Miocene (Serravalian-Tortonian)

Aissaoui (1984)	N145 -152
Ben ayed (1986)	N140 -150
Ben Ferjani et al., (1990)	N140
Bouaziz (1995)	N130
Bouaziz et al., (2002)	N130
Bracène et al., (2002)	N130
Burollet (1956)	N140 -150
Dlala (1995)	N130 -140
Dracène et Frizon (2002)	N135 W
Hlaiem (1998)	N120 -130
Gharbi et al., (2014)	N134
Kadri (1988)	N130 -140
Ouali (1984)	N135
Patriat et al., (2003)	N130 -140
Philip et al., (1986 & 1987)	N140 -180
Rouvier (1997)	N135
Yaïch (1984)	N135
Zargouni (1986)	N160
Zouari (1995)	N010 -030

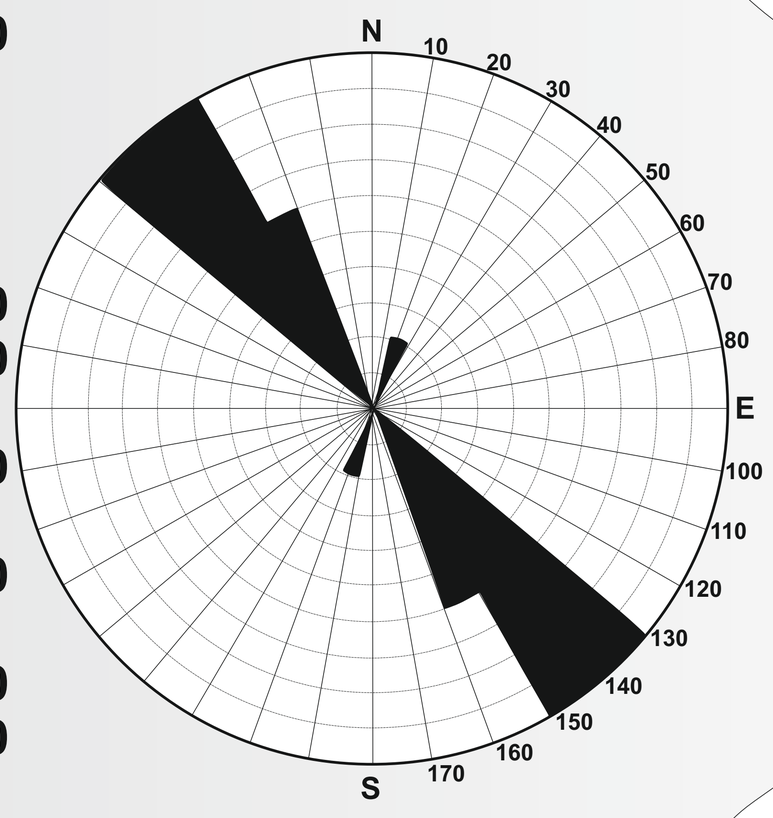

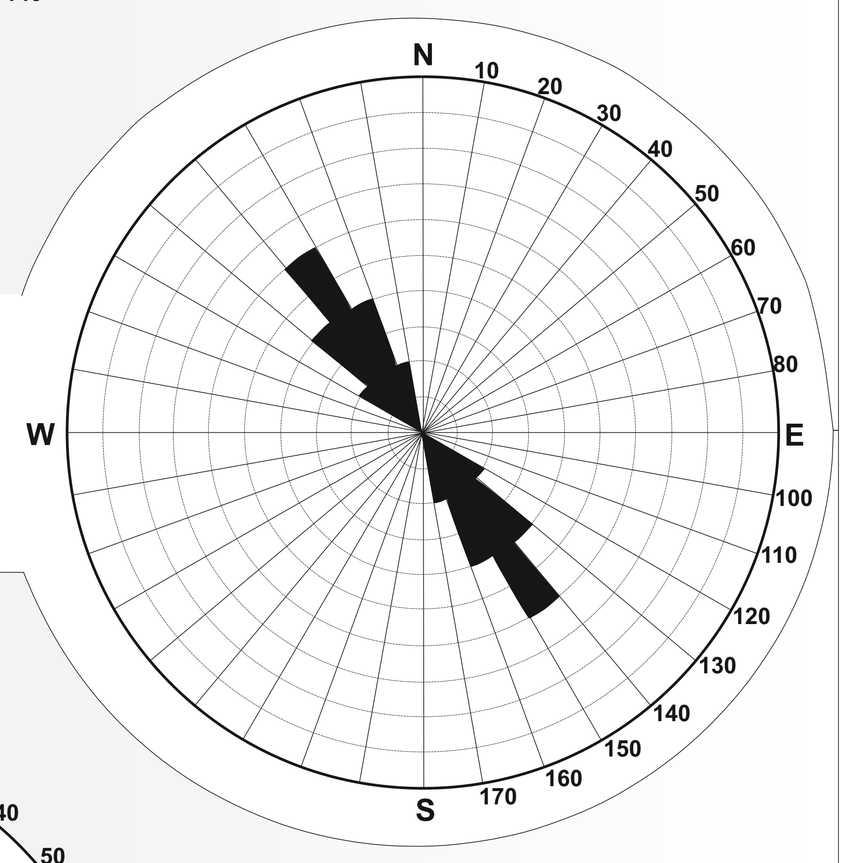

3. Minor phases: Pliocene

Addoum (1995)	N120-150
Aissaoui (1984)	N140-160
Philip et al., (1986)	N130-140

4. Major phases: Quaternary (post-Villafranchian)

Addoum (1995)	N120-150
Ben Ayed (1986)	N160-170
Bouaziz (1995)	N130, N100
Bouaziz et al., (2002)	N150-160
Bracène et Frizon (2000)	N000
Delteil (1982)	N135
Ouali (1984)	N170
Patriat et al., (2003)	N170
Perthuisot (1977)	N120
Philip et al., (1986)	N130-140
Vially et al., (1994)	N000-170
Yaïch (1984)	N135
Zargouni (1986)	N180
Zouari (1995)	N160

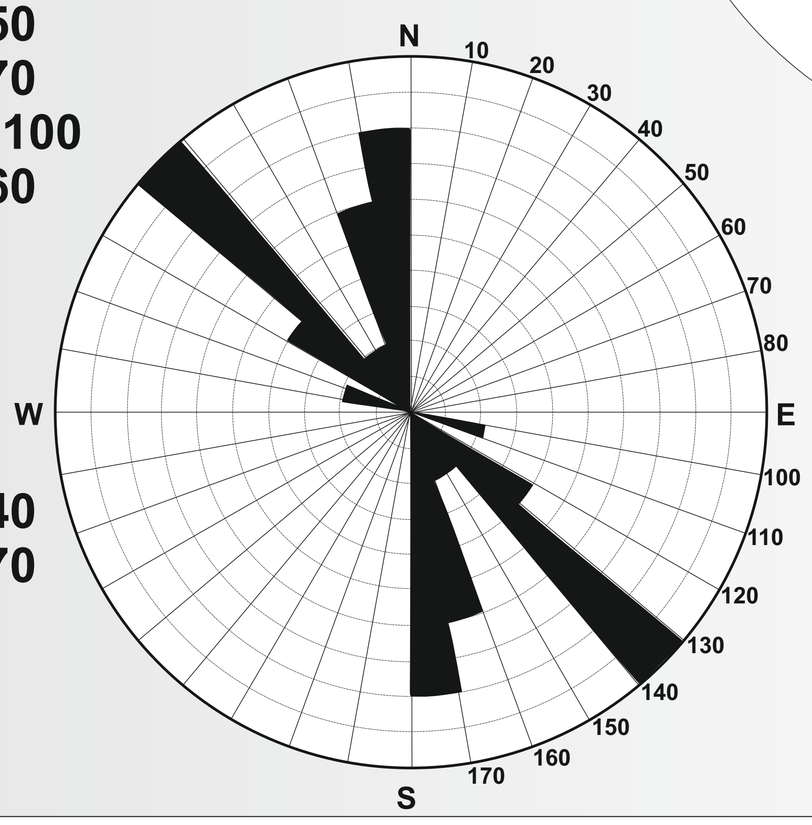

5. Minor phases: actual

Addoum (1995)	N000
Bouaziz (1995)	N030,N120-130
Bouaziz et al., (2002)	N130
Bouaziz et al., (2003)	N130-140
Ben Ferjani et al., (1990)	N150-160
Delteil (1982)	N170-180,N045
Letouzey et Trémolière (1980)	N160
Dlala et Hfaïdh (1989)	N135
Swezey (1996)	N170-180,N130-150
World stress Map (2005)	N150-160
Yaïch (1984)	N170-000
Zouari (1995)	N150

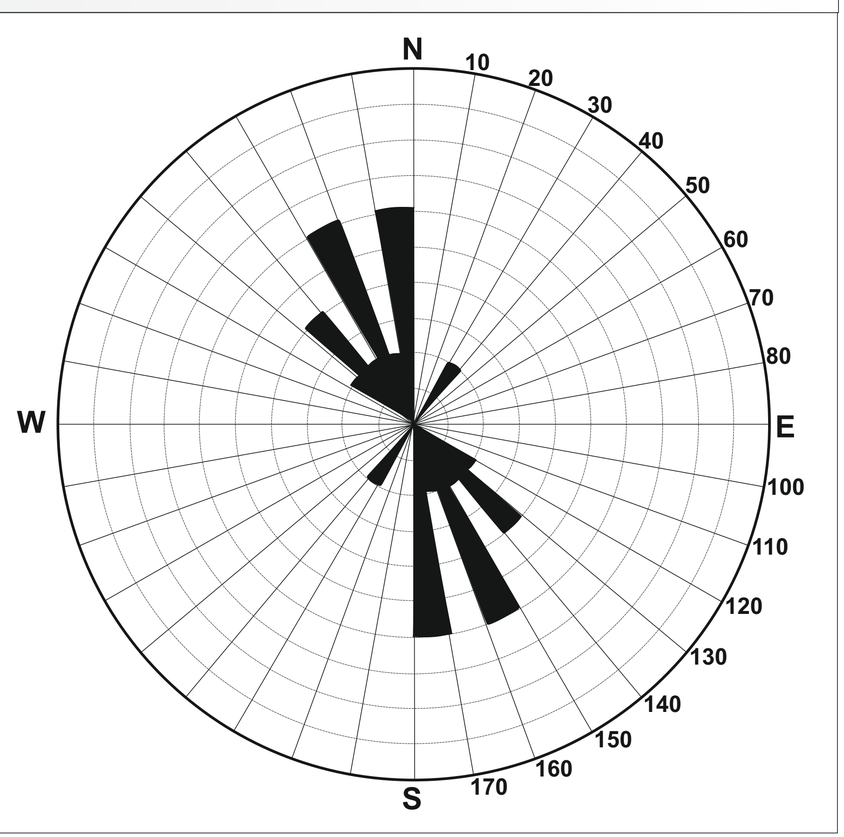

Chronostratigraphy			S (Landward) — Lithostratigraohy — N (Seaward)
QUATERNARY		PLEISTOCENE VILLAFRANCHIAN	Red Beds / Caliche
NEOGENE	PLIOCENE	PIACENZIAN ZANCLEAN	Segui Fm. — Porto Farina Fm. — Raf Raf Fm.
	MIOCENE	MESSINIAN TORTONIAN SERRAVALLIAN	O. Bel KhedimFm. — Somaa Fm. — Melquart Fm. — Kechabta / O.Melah — Oum Douil Fm. — Hakima — Beglia Fm. — Saouaf Fm. — Zelfa Fm. — Birsa Fm.
		LANGHIAN	Ain Ghrab Fm.
		BURDIGALIAN	Messiouta Fm — O. Hammam Fm — Remla Fm — Salaambo Fm — Numidian Flysch
		AQUITANIAN	Fortuna Fm — Ketatna Fm
PALEOGENE	OLIGOCENE	CHATTIAN	Vascus Horizon
		REPULIAN	
	EOCENE	PRIABONIAN	Bouloufa Fm. — Tanit Fm. — Jebs Fm. — Halk ElMenzel Fm. — Souar Fm.
		BARTONIAN	ElHaria Fm.
		LUTETIAN	Metlaoui — Faid Fm. — ElGueria Fm. — Bou Dabouss Fm.
		YPRESIAN	Chouabine Fm.
	PALEOCENE	THANETIAN	Tselja Fm.
		DANIAN	ElHaria Fm.
CRETACEOUS	Upper	MAASTRICHTIAN	Berda Fm. — Abiod Fm. — Merfeg Fm. — Abiod Fm.
		CAMPANIAN	Kef Fm.
		SANTONIAN	Aleg Fm. — Douleb Fm.
		CONIACIAN	Beida Fm. — Bireno Fm.
		TURONIAN	Bahloul Fm.
		CENOMANIAN	Zebbag Fm. — Isis — Upper Fahdene Fm. — Lower Fahdene Fm.
	Lower	ALBIAN	Orbata Fm. — Serj Fm.
		APTIAN	Sidi Aich Fm.
		BARREMIAN	Bouhedma Fm. — Mrihla Fm.
		HAUTERIVIAN	Boudinar Fm.
		VALANGINIAN	Asfer Group — Meloussi Fm. — Sidi Khalif Fm.
		BERRIASIAN	

Tectonic events

ATLASIC — ALPINE

PYRENEAN

Hauterivian - Lower Barremian

Bouhedma

Upper Barremian

Sidi Aich Fm.

Aptian

Orbata Fm.

Age

Form.

Thickness (m)

Sedimentary features

Field bservations

BPVs distribution (cm)

dolomite

gypsum

mudstones

marl

Sandstones

BPVs

oblique veins

N° of BPVs

cross-bedding

silicified wood

fishes

bioturbation

bioclast

bivalves

Relative abundance

Thicknesses

Hauterivian - Lower Barremian

Bouhedma.Fm

Fig.10

1m

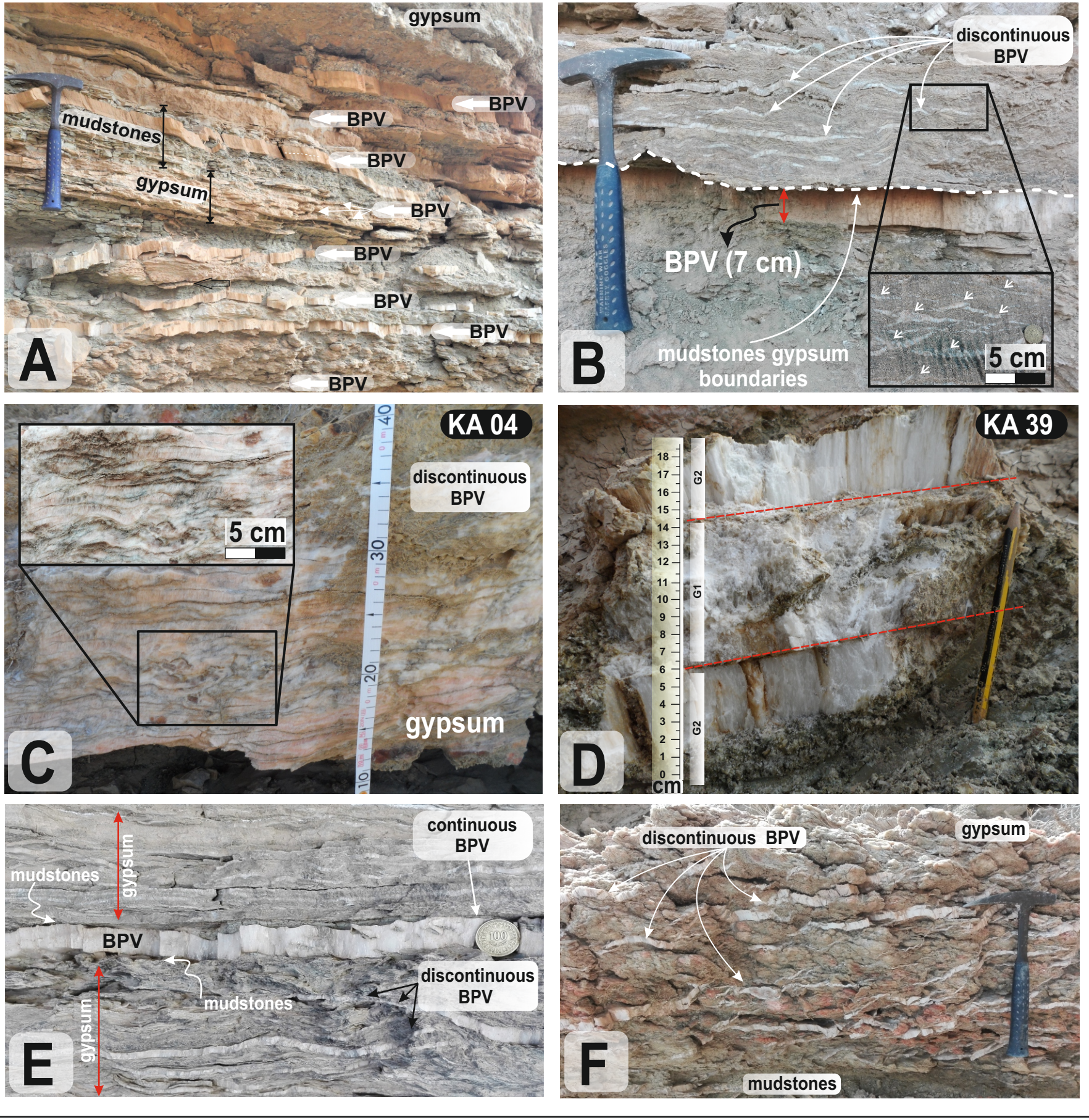
gypsum
BPV
BPV
BPV
BPV
BPV
BPV
BPV
BPV
mudstones
gypsum
A
discontinuous BPV
BPV (7 cm)
mudstones gypsum boundaries
5 cm
B
KA 04
discontinuous BPV
5 cm
gypsum
C
KA 39
G2
G1
G2
cm
D
continuous BPV
mudstones
gypsum
BPV
mudstones
discontinuous BPV
gypsum
E
discontinuous BPV
gypsum
mudstones
F

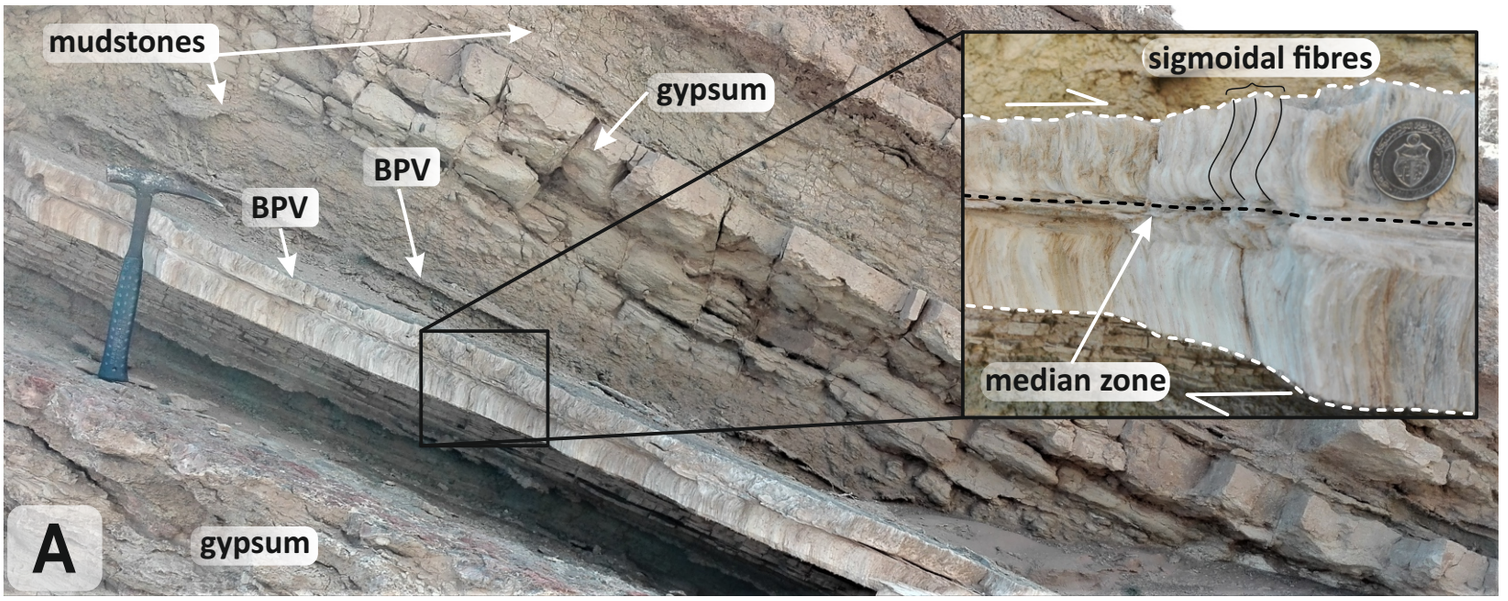
mudstones
gypsum
BPV
BPV
sigmoidal fibres
median zone
A
gypsum

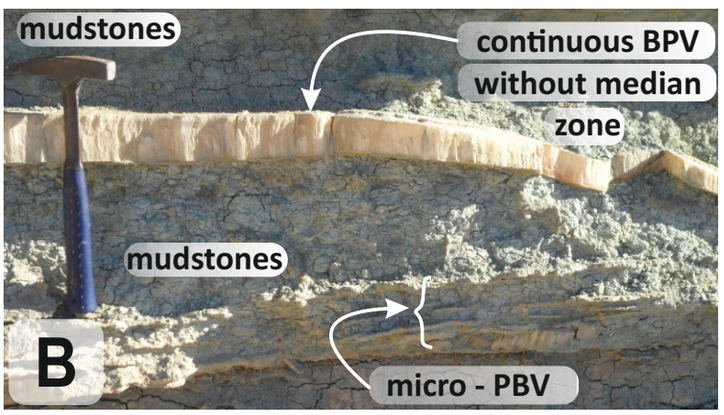
mudstones
continuous BPV
without median
zone
mudstones
B
micro - PBV

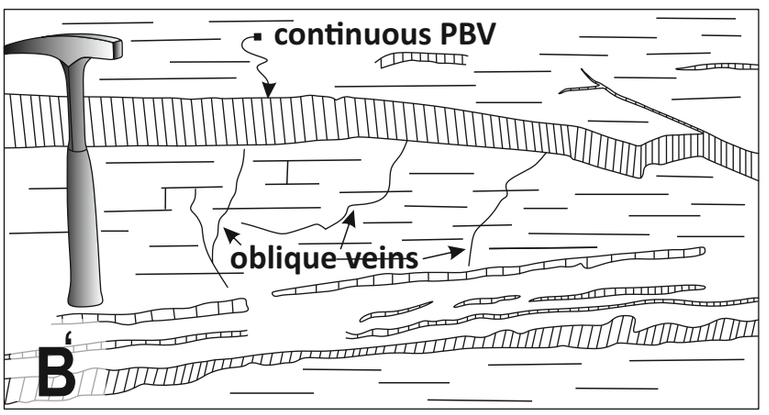
continuous PBV
oblique veins
B'

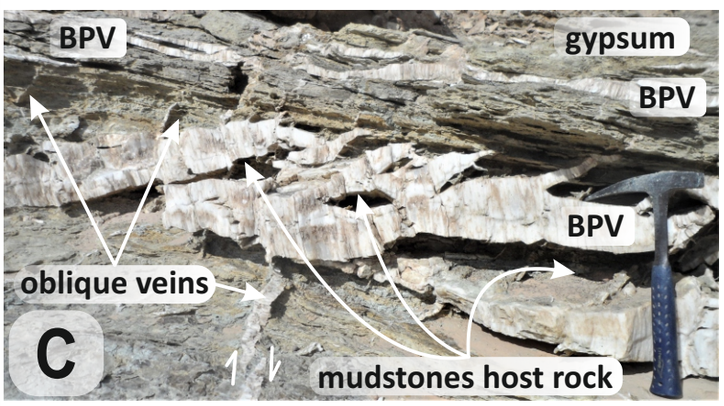
BPV
gypsum
BPV
BPV
oblique veins
C
mudstones host rock

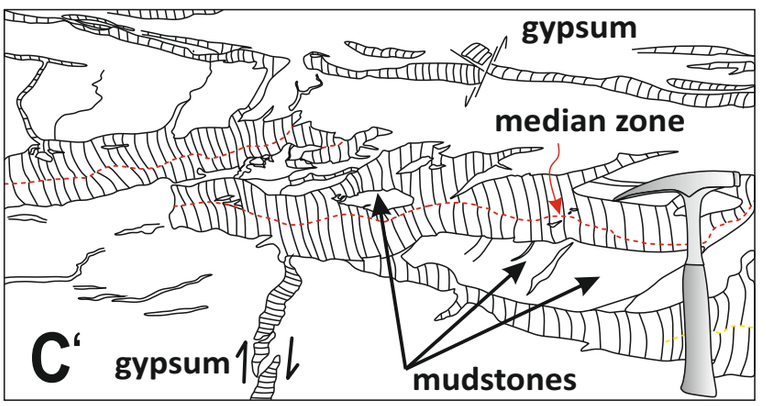
gypsum
median zone
C'
gypsum
mudstones

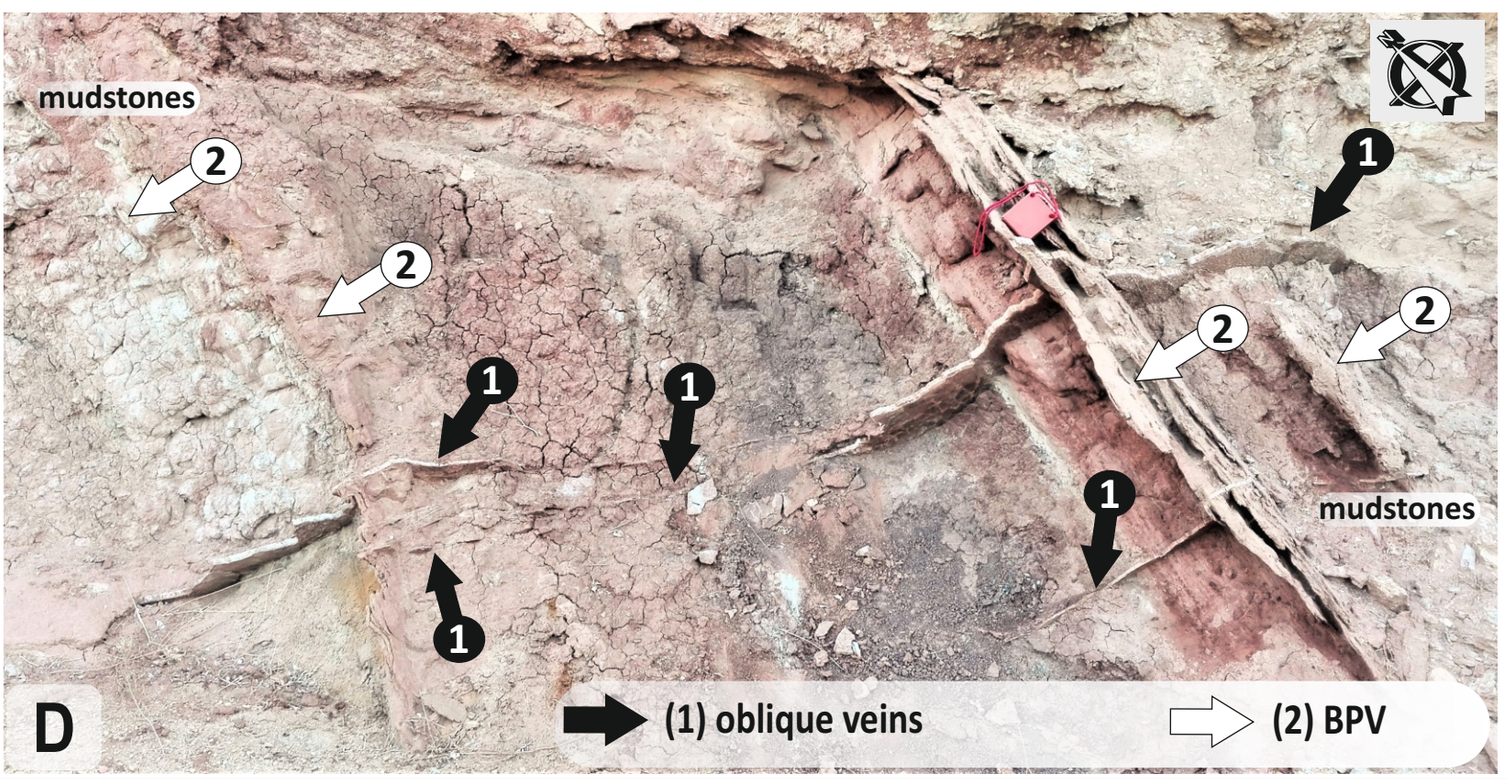
mudstones
2
2
1
1
1
2
2
1
1
mudstones
D
(1) oblique veins
(2) BPV

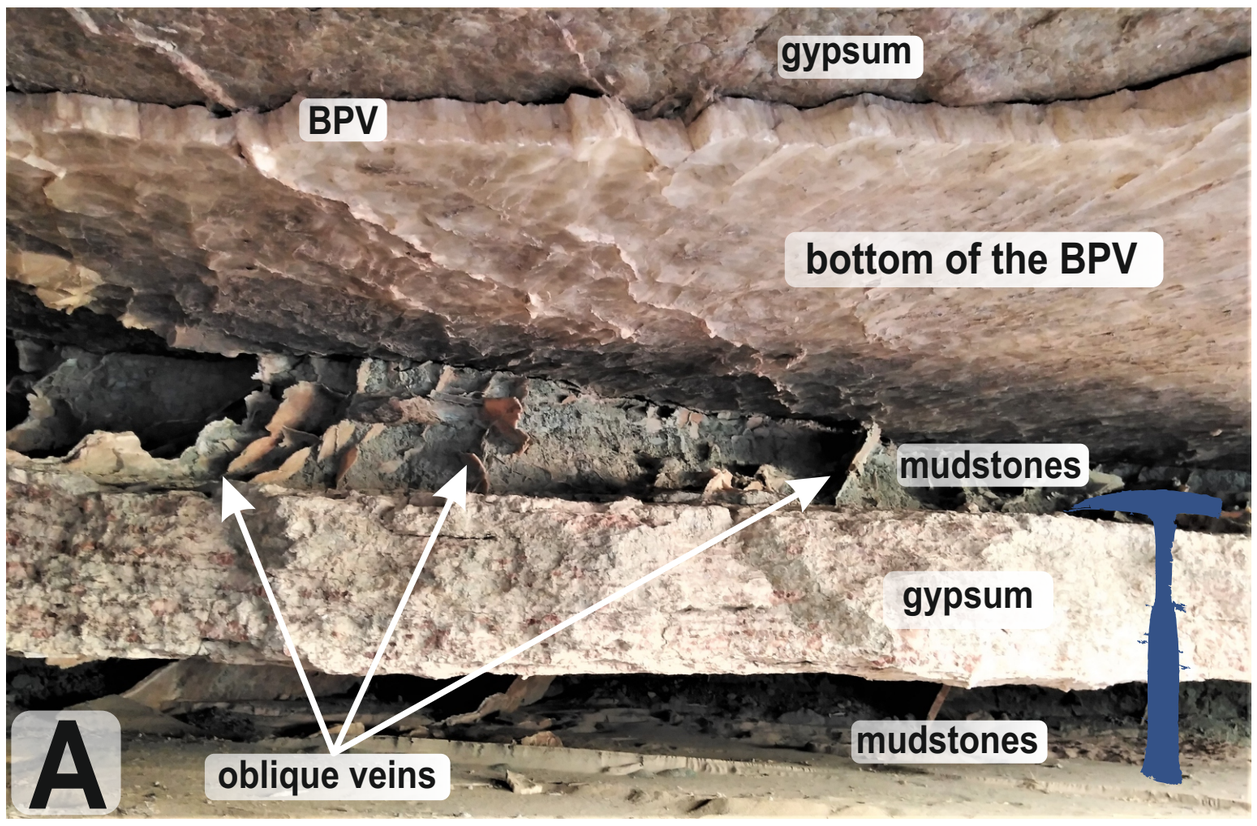
gypsum
BPV
bottom of the BPV
mudstones
gypsum
mudstones
oblique veins
A

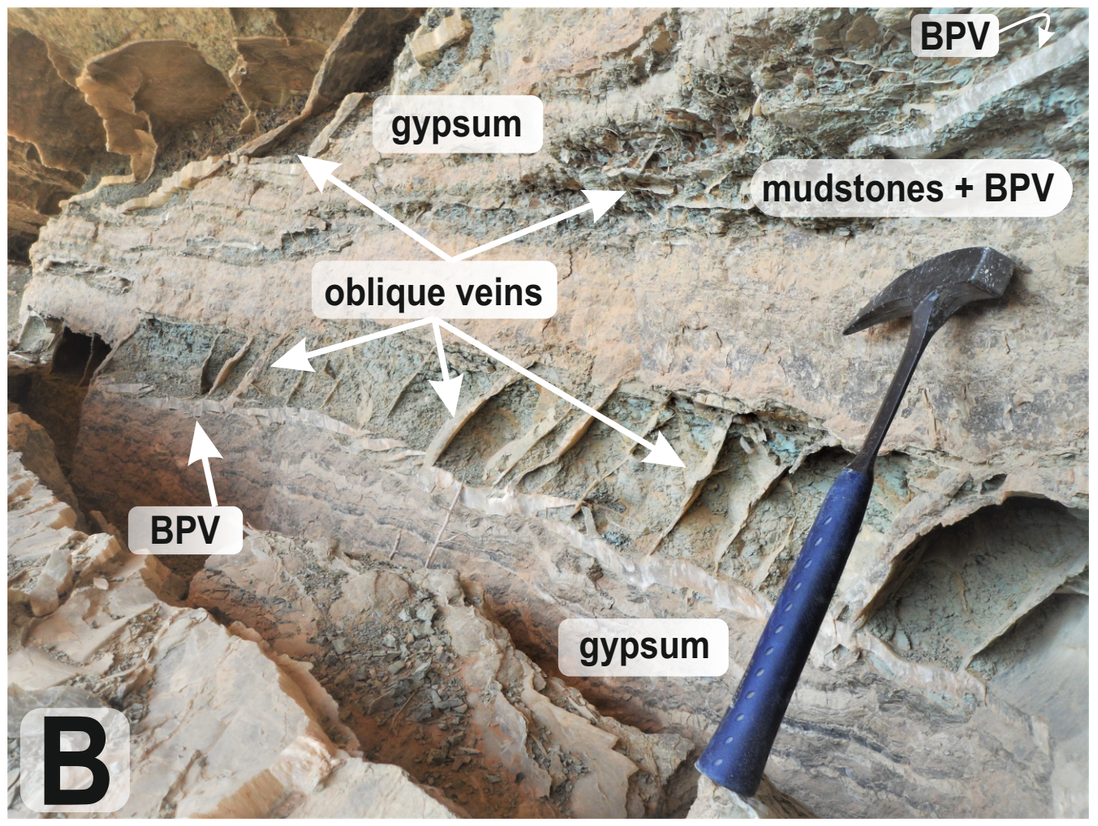
BPV
gypsum
mudstones + BPV
oblique veins
BPV
gypsum
B

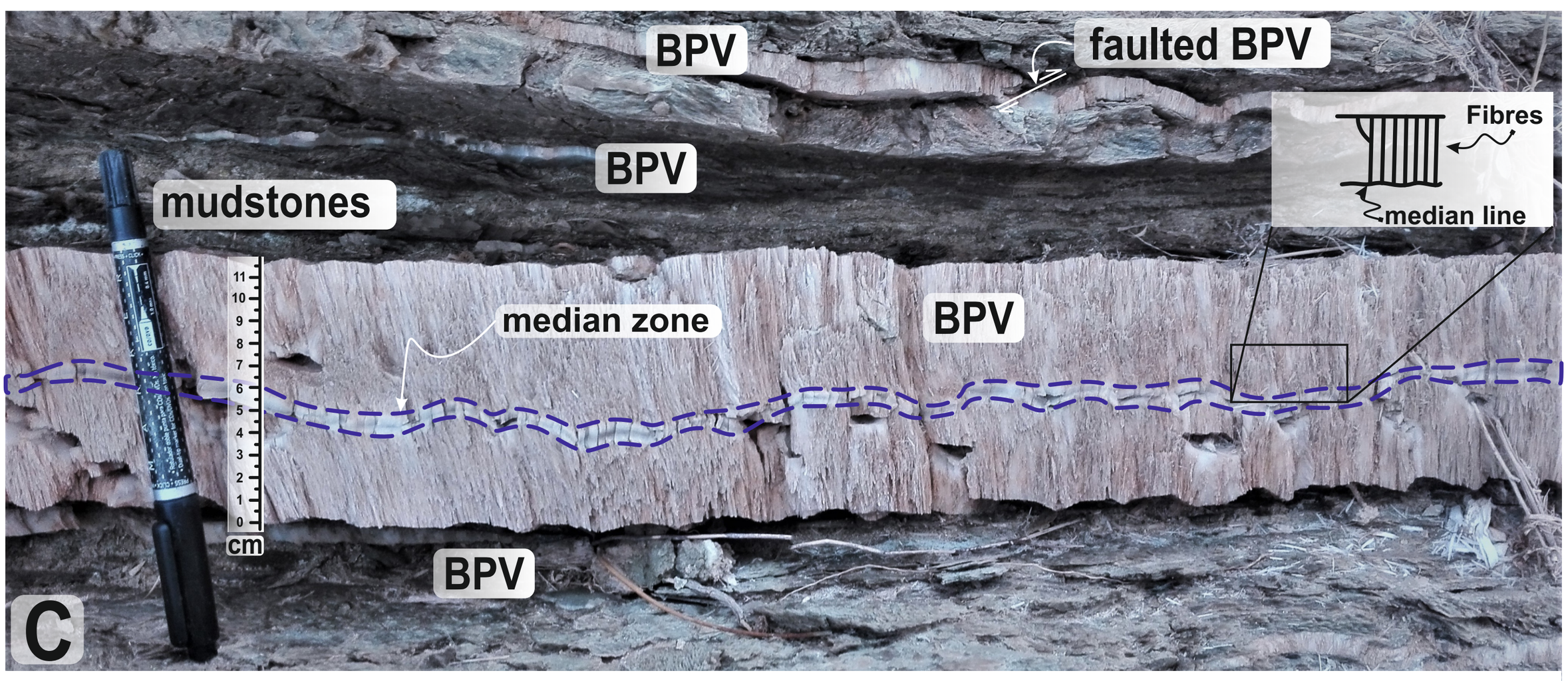
BPV
faulted BPV
Fibres
median line
BPV
mudstones
median zone
BPV
11
10
9
8
7
6
5
4
3
2
1
0
cm
BPV
C

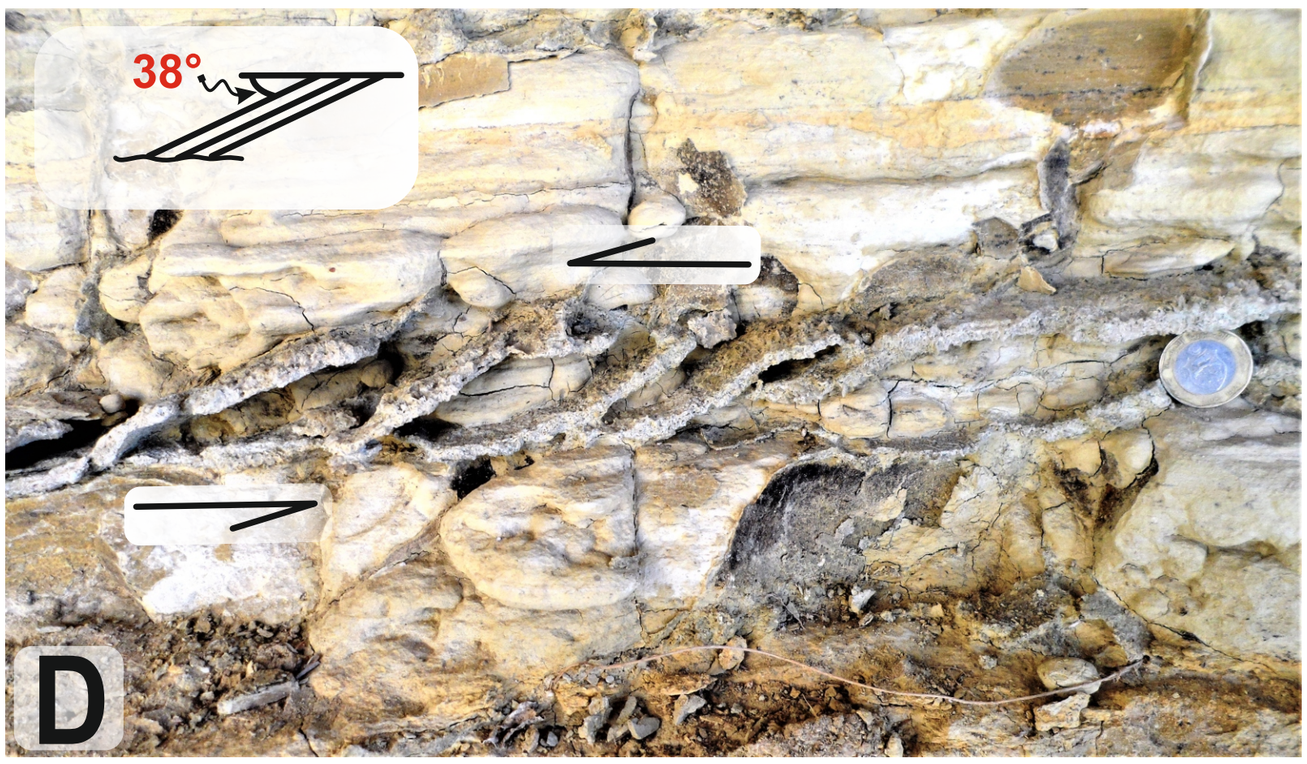
38°
D

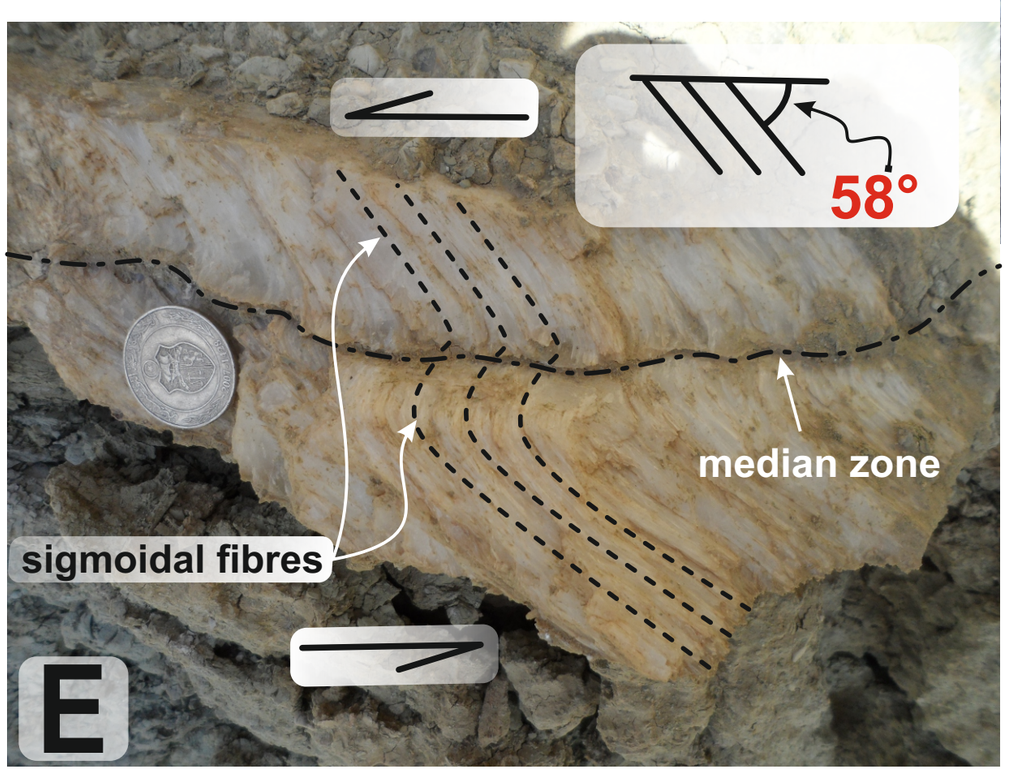
58°
median zone
sigmoidal fibres
E

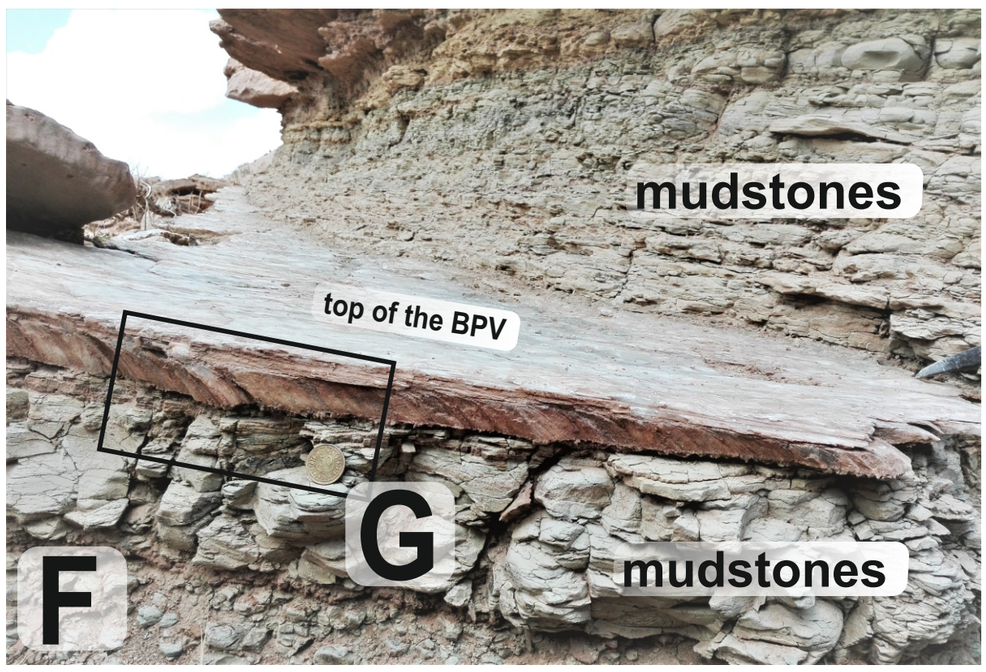
mudstones
top of the BPV
G
F
mudstones

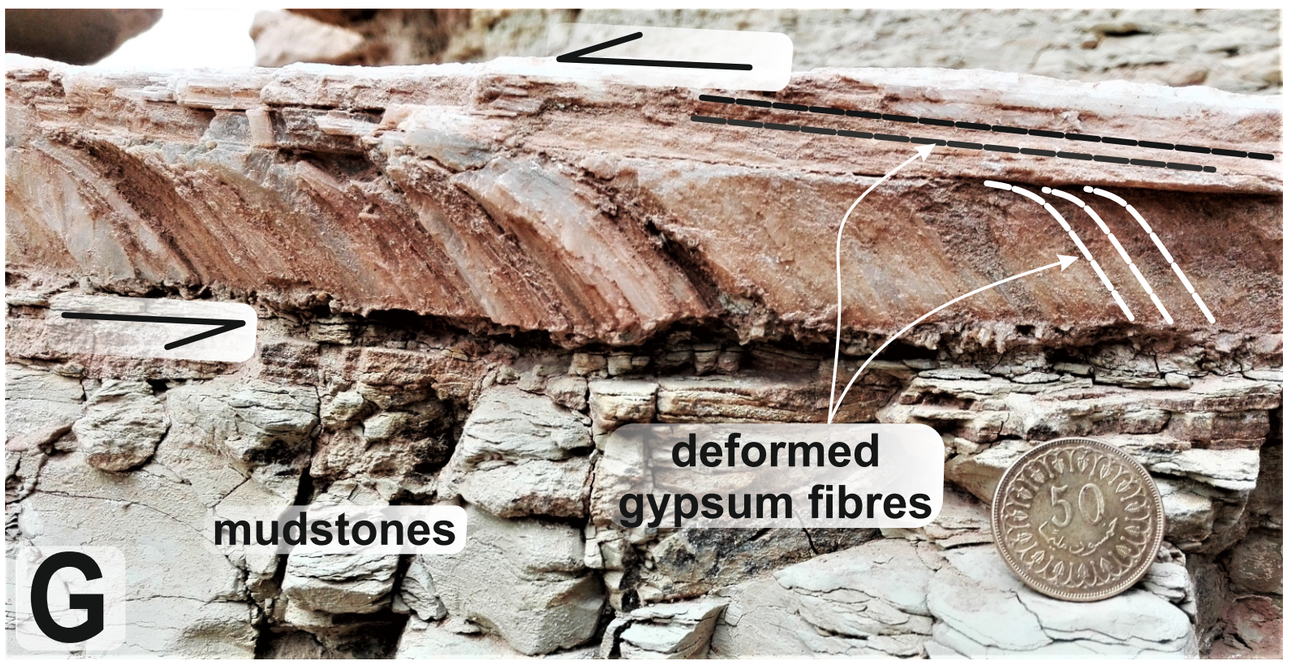
deformed
gypsum fibres
mudstones
G

Ka01

Ka12

Ka14

Ka17

Ka04

PAL

NL

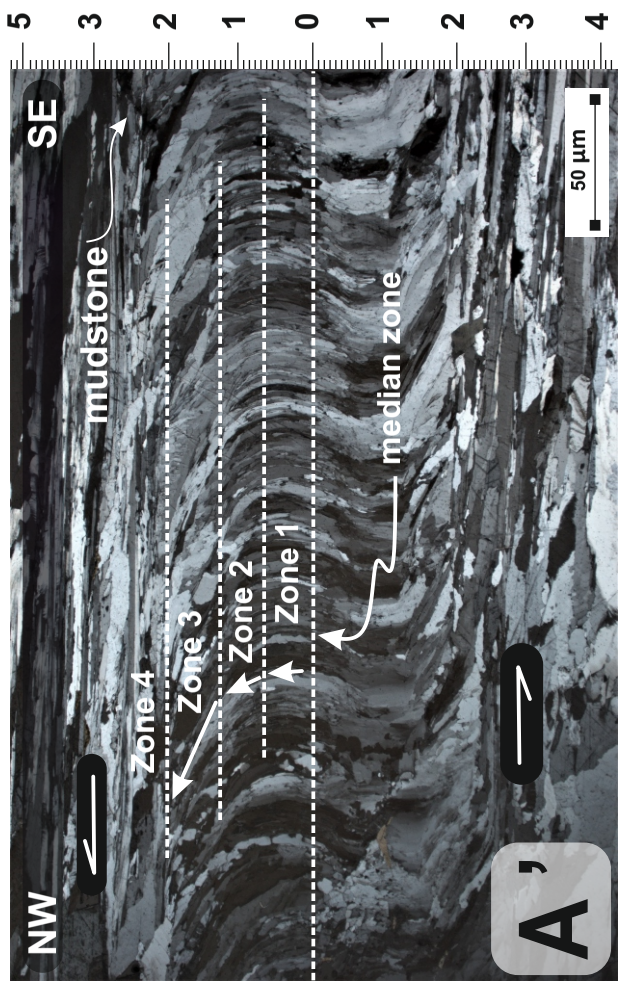

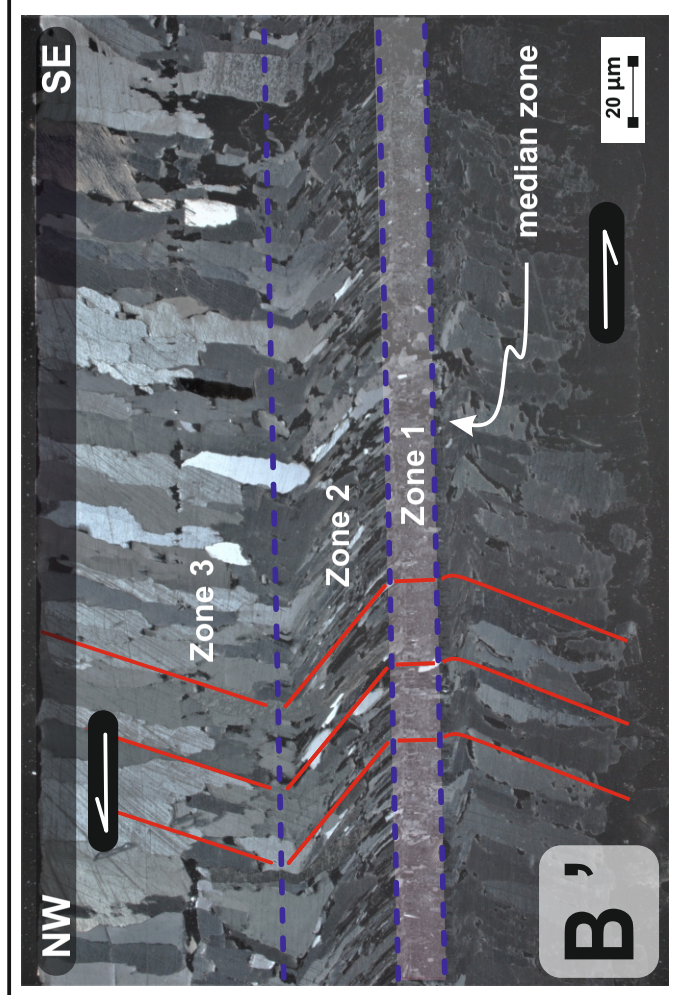

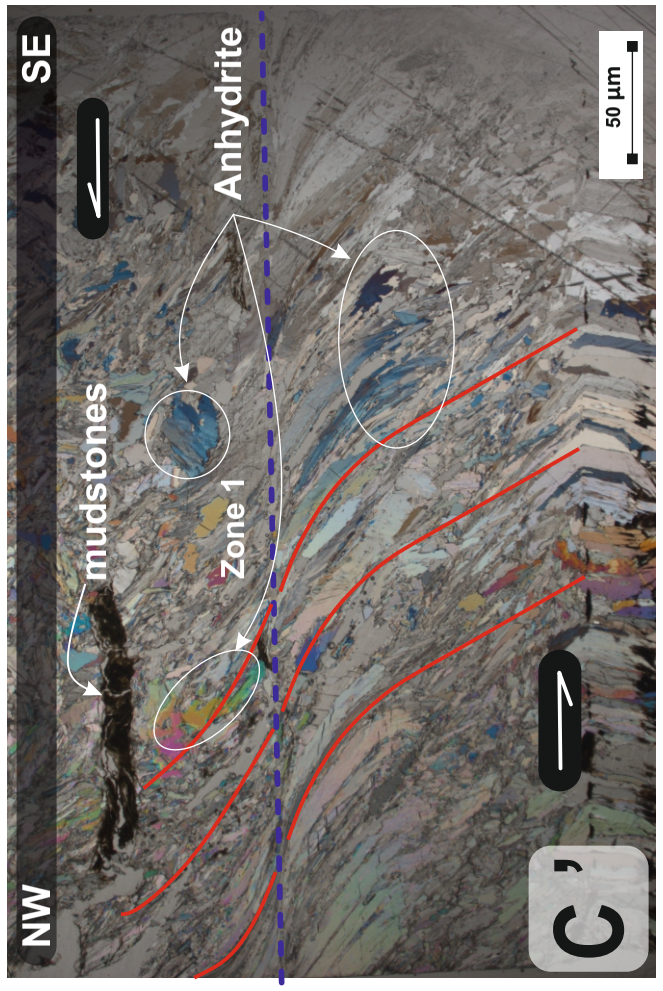

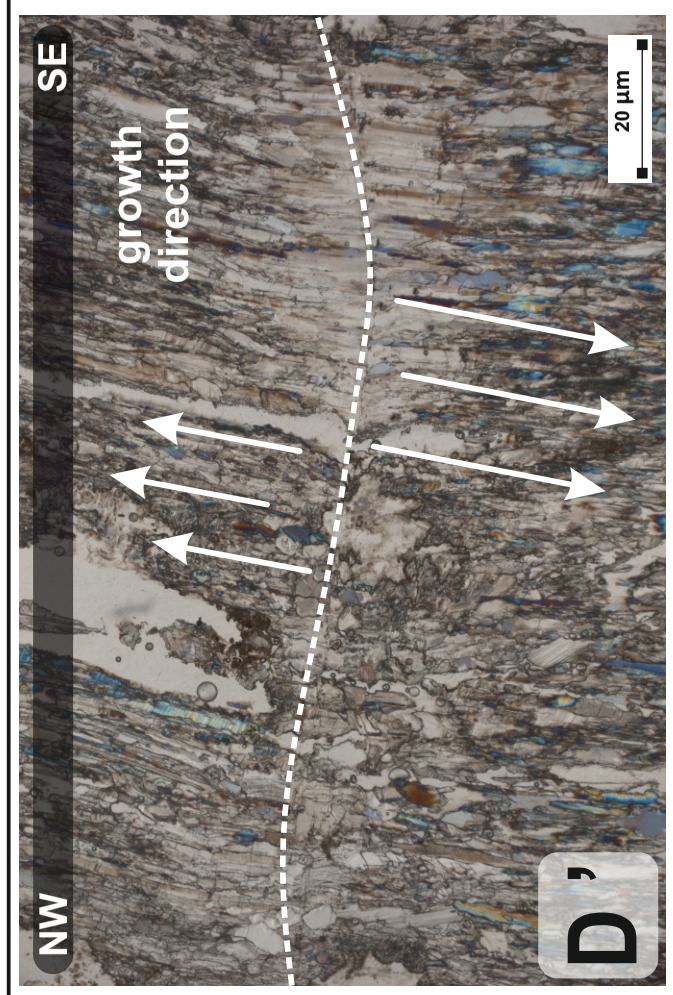

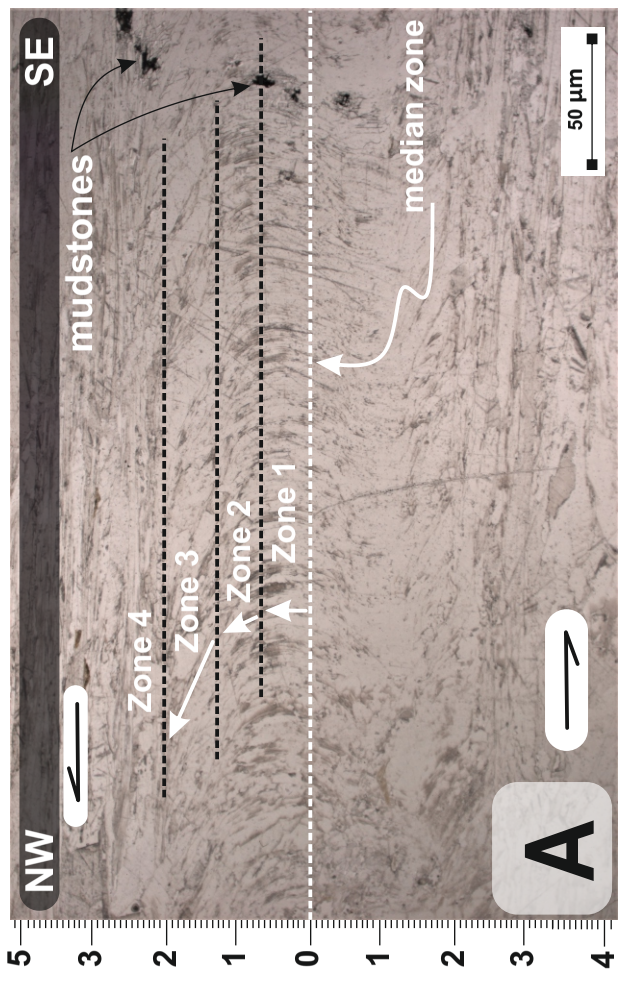

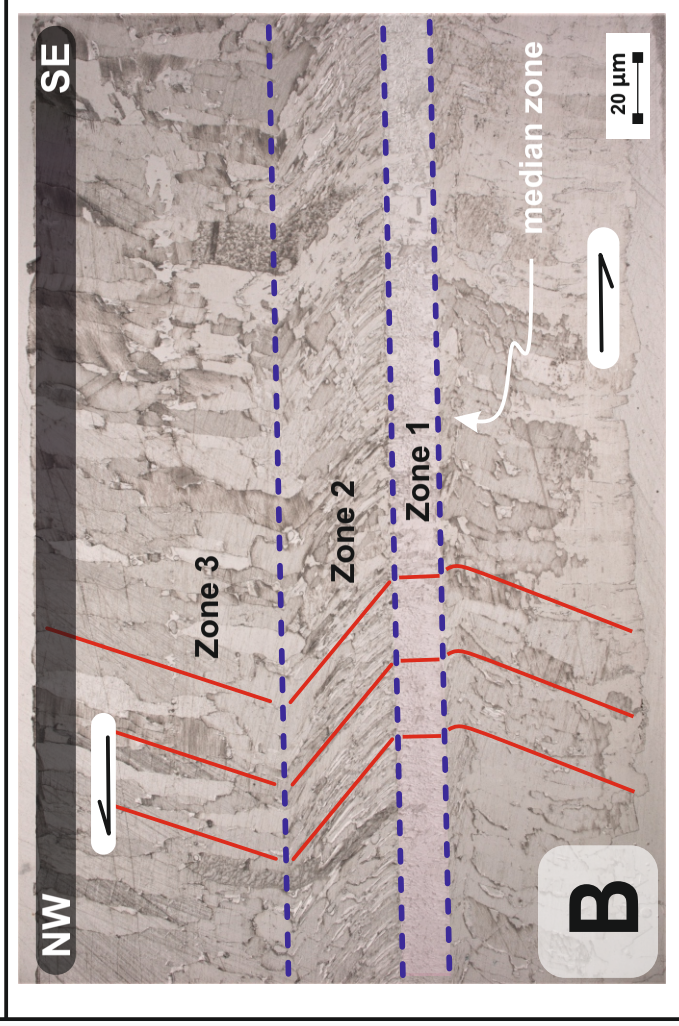

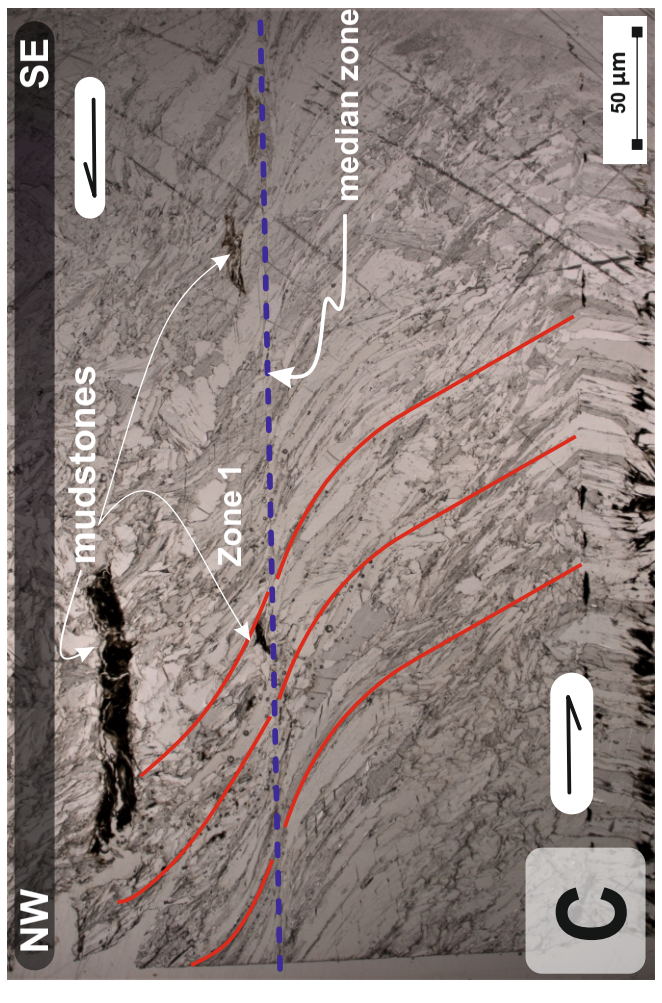

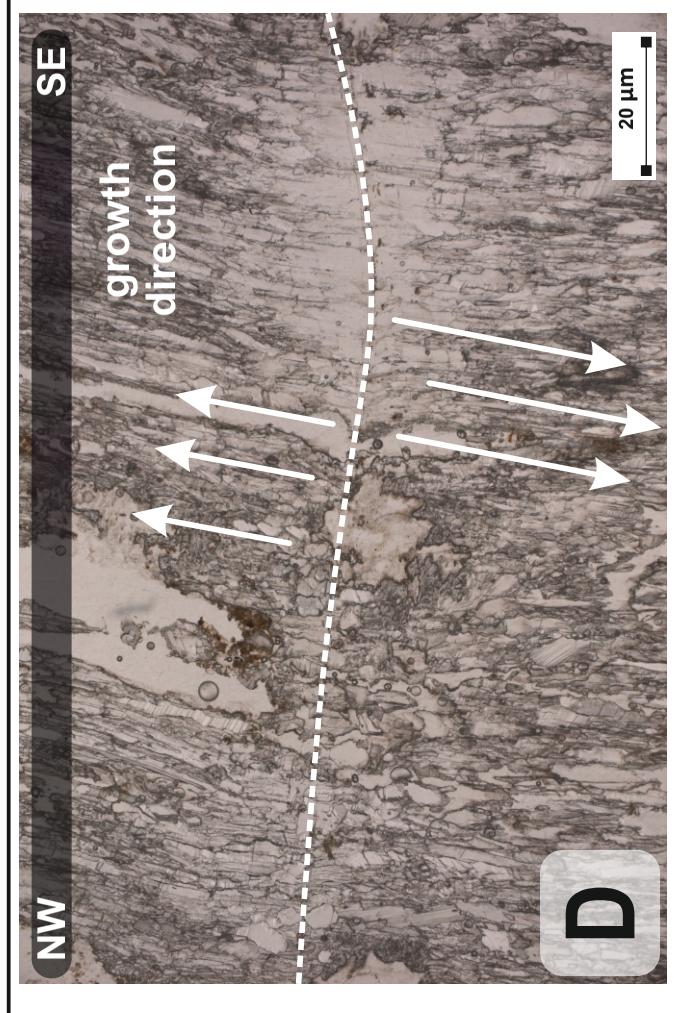

Host rock

Mudstones

Evaporite

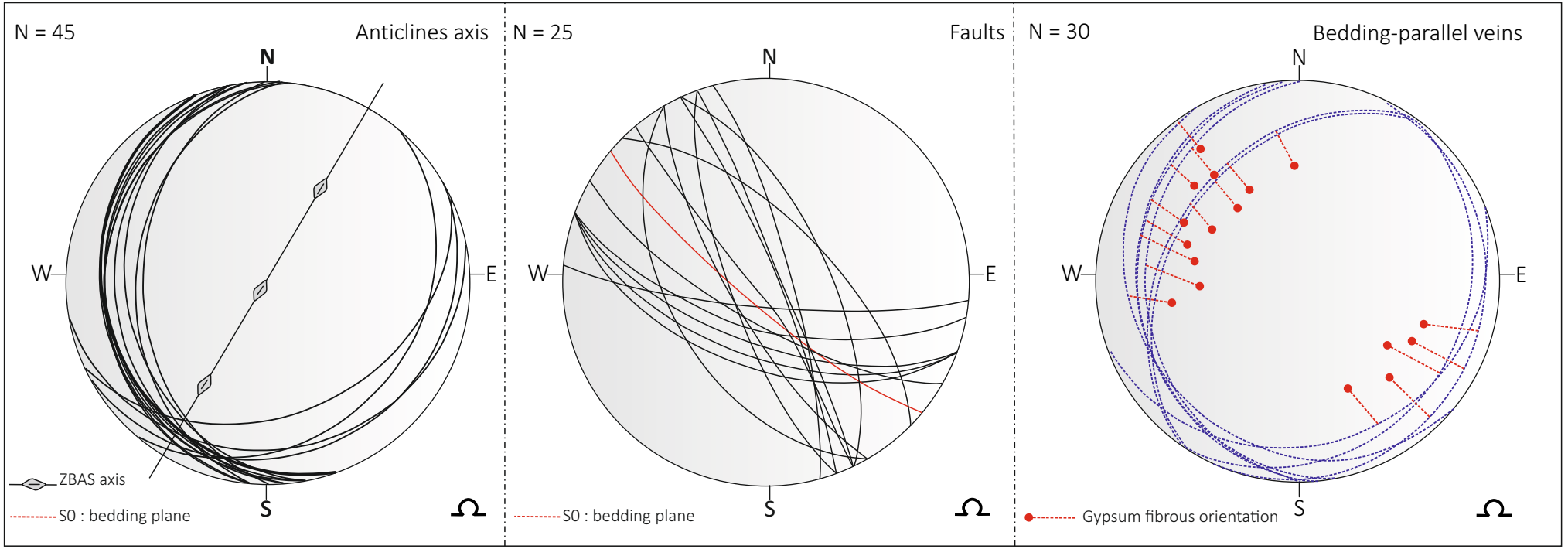
N = 45
Anticlines axis
N
W
E
S
ZBAS axis
S0 : bedding plane
N = 25
Faults
N
W
E
S
S0 : bedding plane
N = 30
Bedding-parallel veins
N
W
E
S
Gypsum fibrous orientation

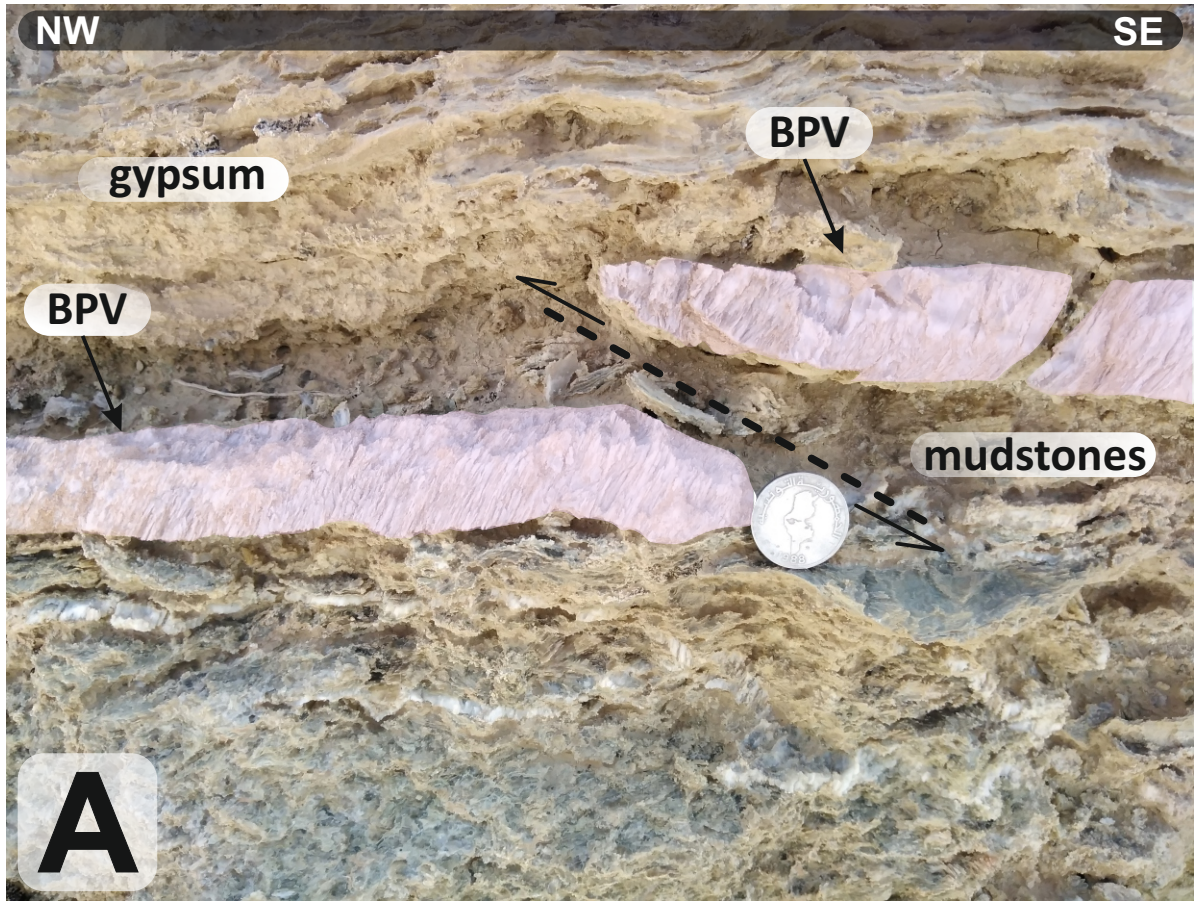
NW
SE
gypsum
BPV
BPV
mudstones
A

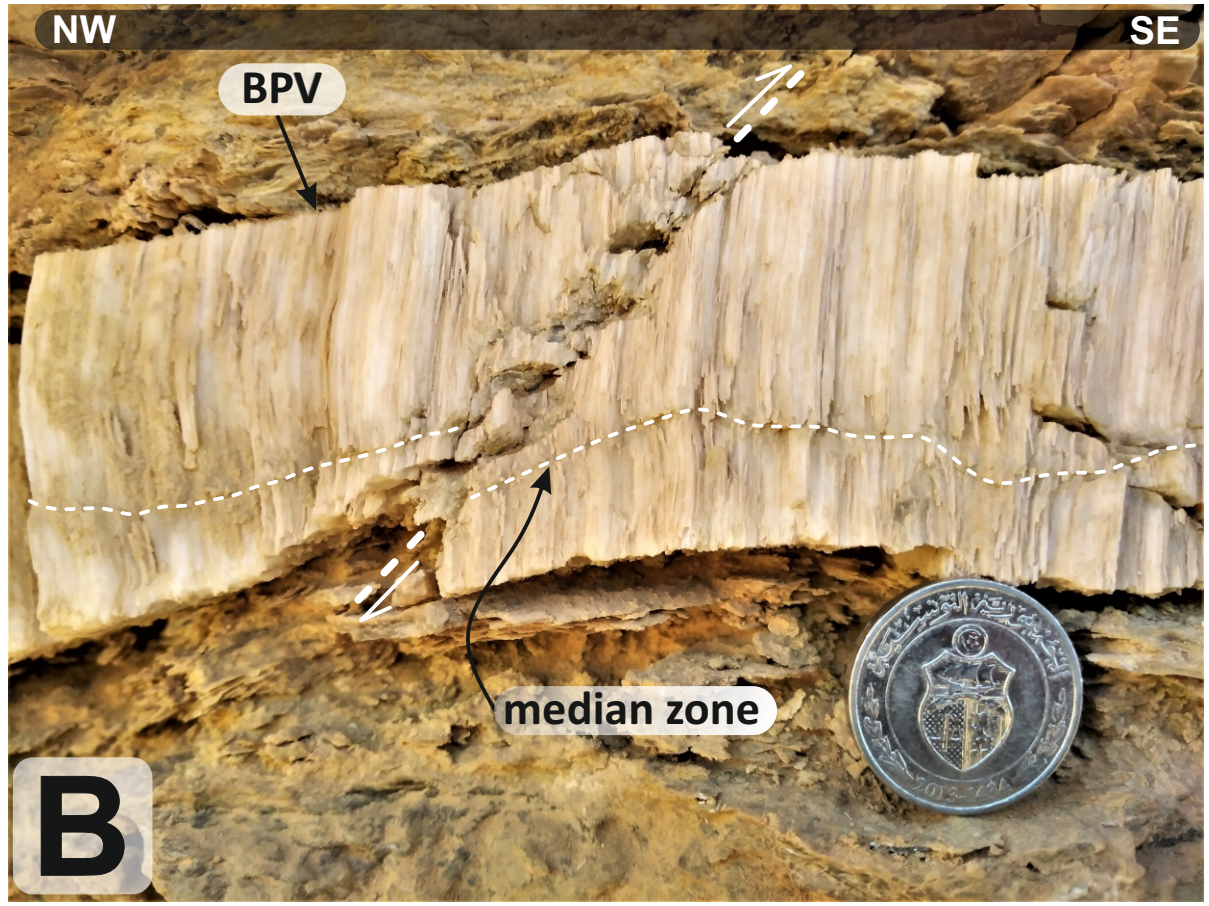
NW
SE
BPV
median zone
B

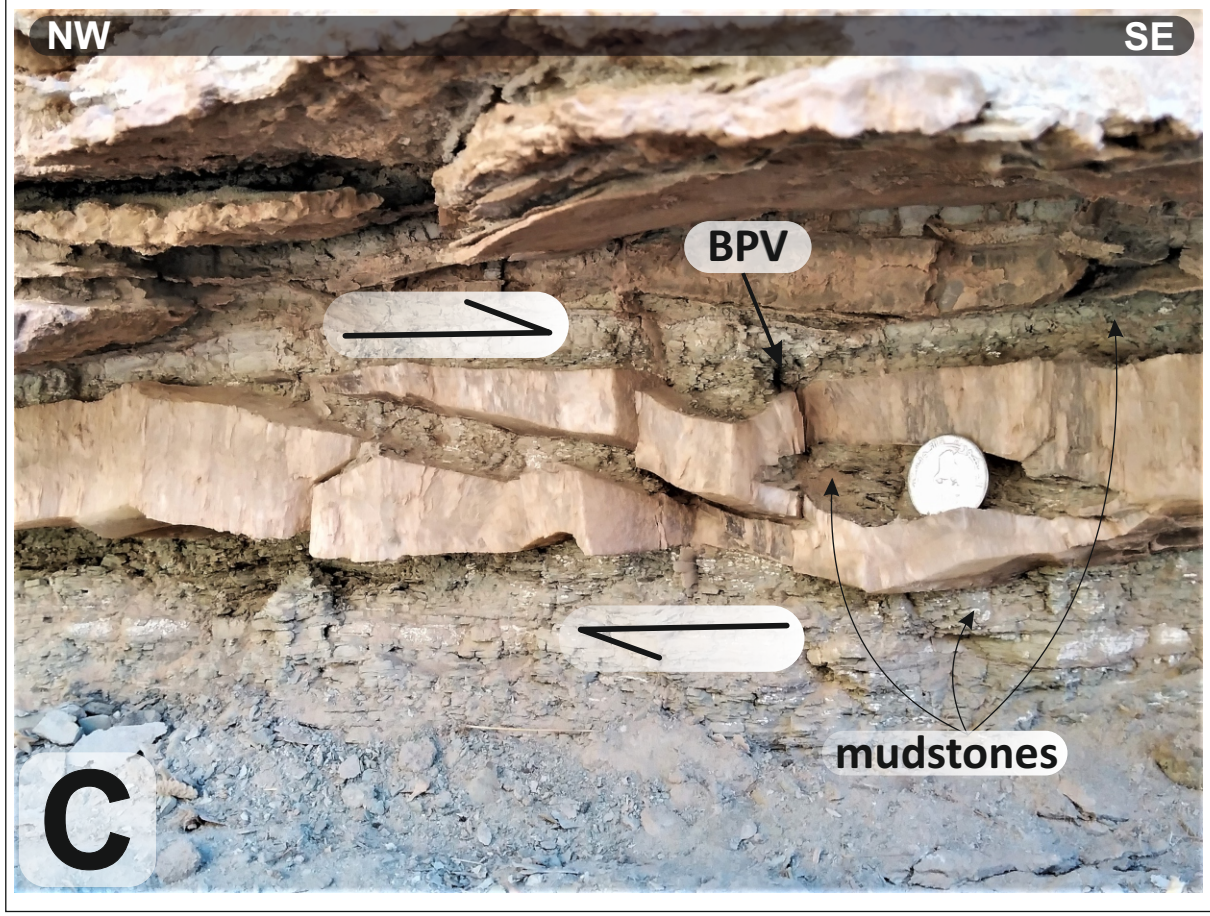
NW
SE
BPV
mudstones
C

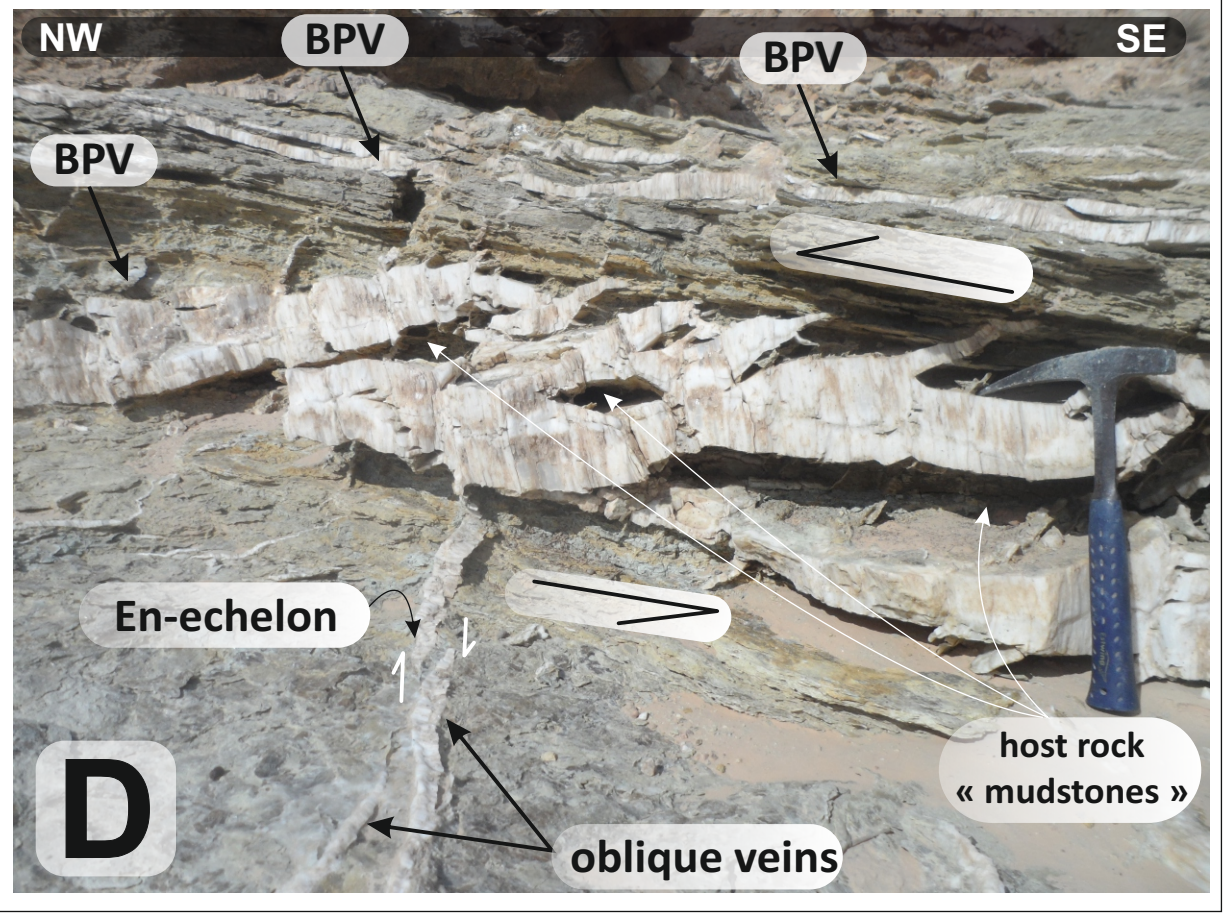
NW
SE
BPV
BPV
BPV
En-echelon
host rock
« mudstones »
oblique veins
D

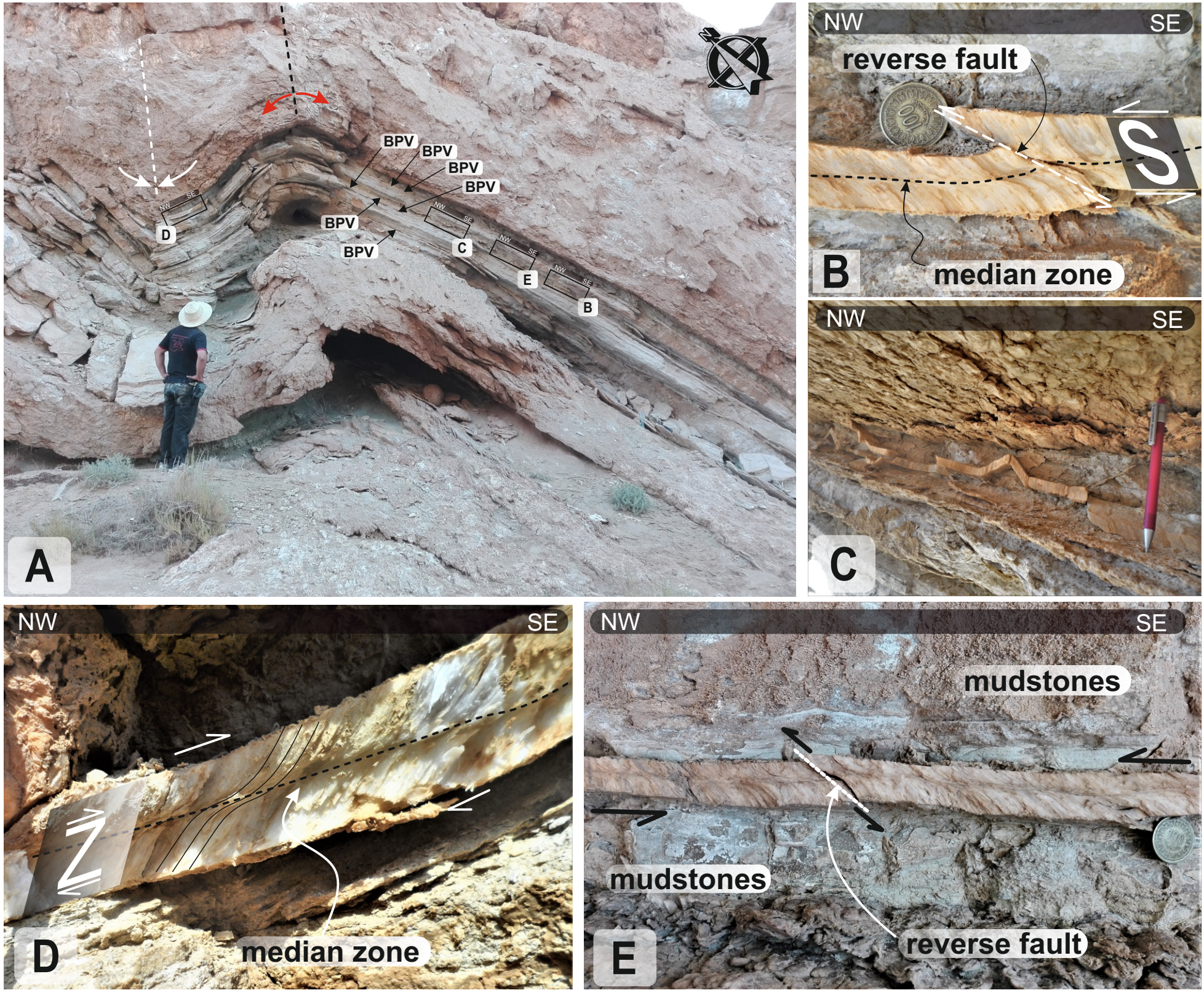
A
BPV
BPV
BPV
BPV
BPV
BPV
D
C
E
B
NW
SE
B
reverse fault
median zone
C
D
median zone
E
mudstones
mudstones
reverse fault

1. Initial stage : depostion

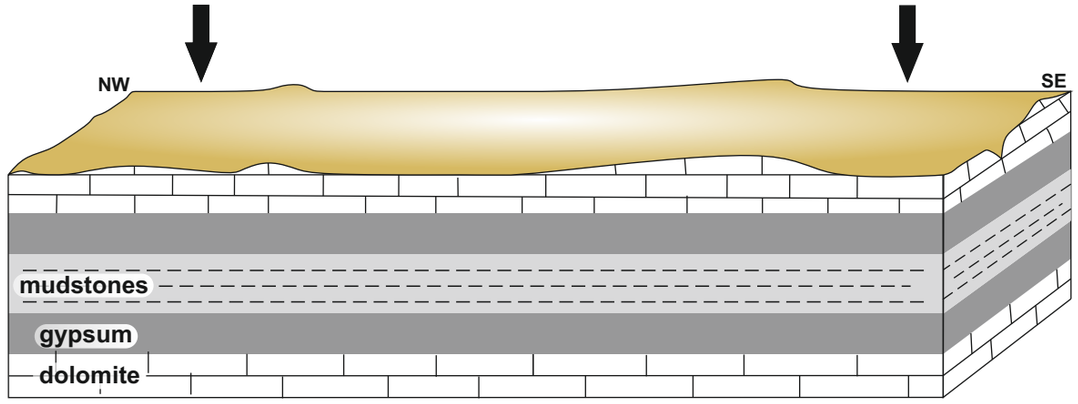

2 .First generation of BPVs with undeformed fibres

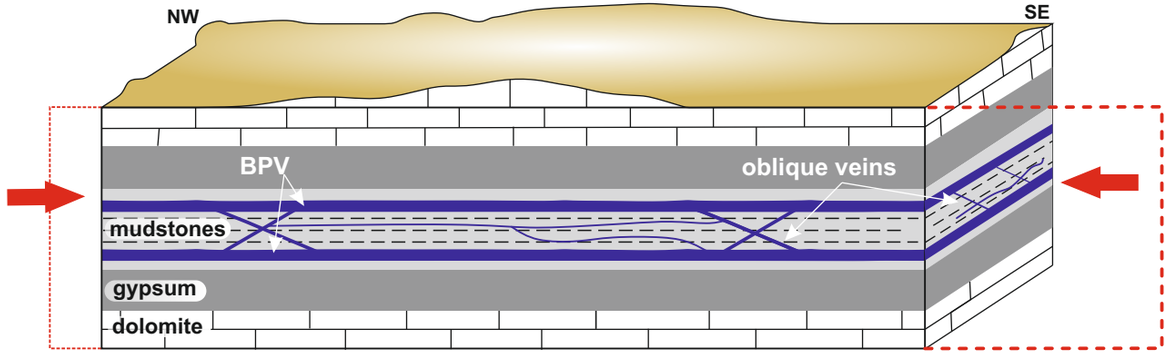

3 . Shortening during Miocene: generation of BPVs with curved fibres, ‘ en-échelon ’ structures, filled fractures, folds and faults.

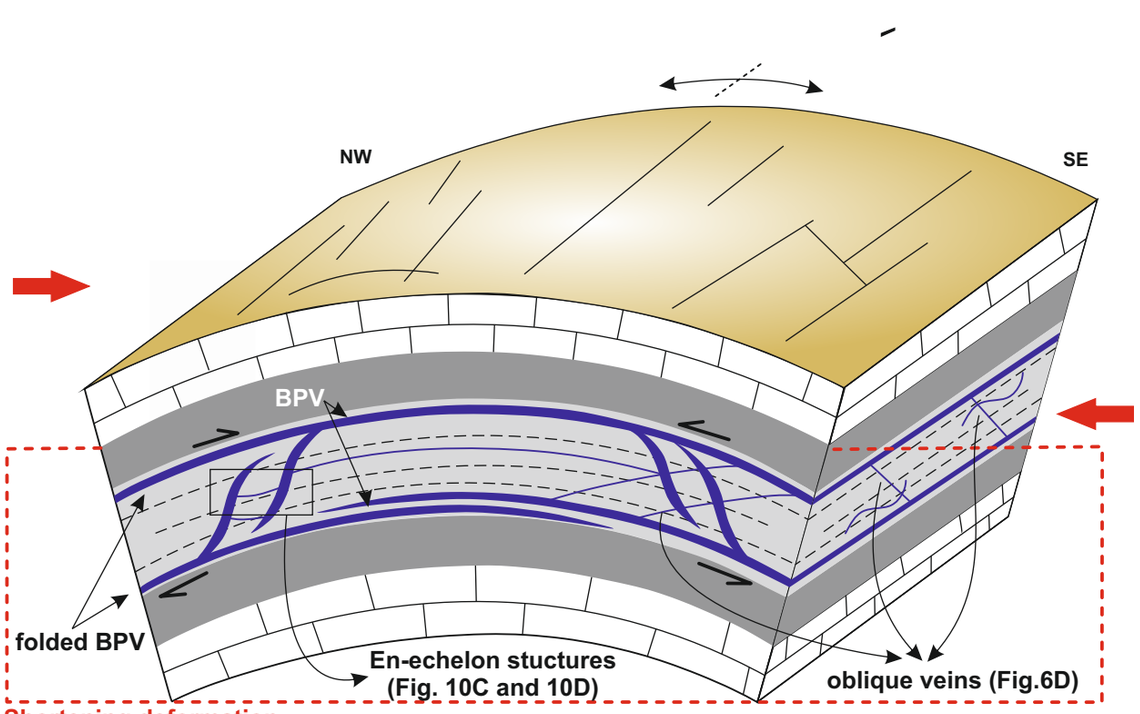

4 . Folding during post-Villanfranchian : generation of BPVs with curved fibres and oblique filled fractures corss-cutting the first stage

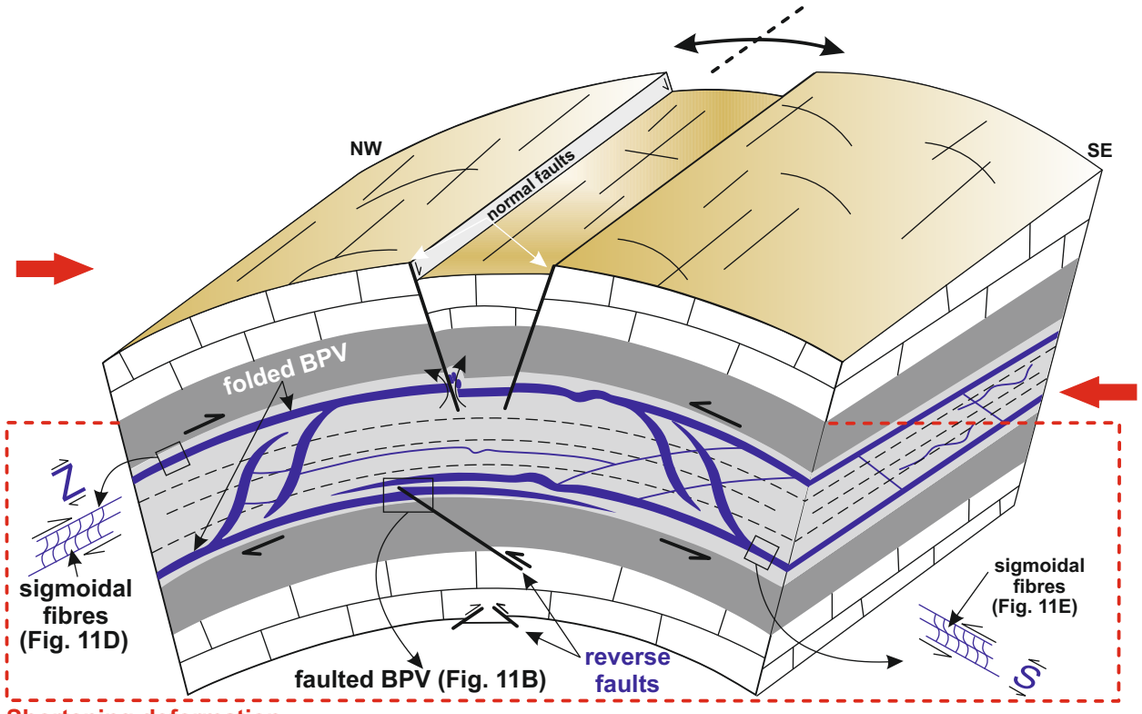

Sample N°	*Length (cm)*	*Width (m)*	*Ratio*	*Bedding plane (S0)*	*Host rock*	*GPS*	
						(X)	*(Y)*
KA1	4	3	1,33	N000 00E	Mudstones	9.863910°	34.067012°
KA2	5	5	1	-	Mudstones	9.863931°	34.066976°
KA3	5	2	2,5	N180 17 E	Mudstones	9.863965°	34.066962°
KA4	20	15	1,33	N186 22 E	Evaporite	9.864273°	34.066813°
KA5	2	2,5	0,8	N160 20 NE	Mudstones	9.864374°	34.066804°
KA6	2	2	1	-	Mudstones	9.864645°	34.066899°
KA7	25	26,3	0,95	N170 13 NE	Evaporite	9.864980°	34.066723°
KA8	8	5	1,6	N155 20 NE	Mudstones	9.864970°	34.066726°
KA9	15	35,7	0,43	N165 16 NE	Evaporite	9.864970°	34.066726°
KA10	2	3,2	0,63	N110 20 NE	Mudstones	9.864998°	34.066748°
KA11	2	2	1	N110 20 NE	Mudstones	9.865051°	34.066744°
KA12	50	10	5	-	Evaporite	9.865353°	34.066344°
KA13	50	2	25	-	Mudstones	9.865404°	34.066291°
KA14	50	11	4,55	-	Mudstones	9.865586°	34.066180°
KA15	50	7	7,15	-	Mudstones	9.866027°	34.065691°
KA16	15	15	1	-	Evaporite	9.866067°	34.065644°
KA17	20	2	10	N120 25 NE	Mudstones	9.866065°	34.065632°
KA18	25	28	0,90	-	Evaporite	9.866207°	34.065589°
KA19	50	4	12,5	-	Mudstones	9.866319°	34.065573°
KA20	50	39,4	1,27	-	Evaporite	9.866640°	34.065496°
KA21	50	11	4,55	-	Mudstones	9.866608°	34.065495°
KA22	60	12	5	-	Evaporite	9.866582°	34.065510°
KA23	80	2	40	N174 30 E	Mudstones	9.866544°	34.065513°
KA24	80	2	40	-	Mudstones	9.866480°	34.065544°
KA25	60	3	20	N178 25 E	Mudstones	9.866409°	34.065551°
KA26	80	2	40	-	Mudstones	9.866319°	34.065573°
KA27	80	2	40	N005 72 E	Mudstones	9.865660°	34.066263°
KA28	80	4	20	-	Mudstones	9.865610°	34.066292°
KA29	40	3	13,33		Mudstones	9.865520°	34.066280°
KA30	80	28	2,86	N25 22 E	Evaporite	9.865448°	34.066272°
KA31	80	12	6,67	-	Mudstones	9.865772°	34.066052°
KA32	10	3	3,33	--	Evaporite	9.865764°	34.066089°
KA33	50	2	25	-	Mudstones	9.865713°	34.066120°
KA34	50	4	12,5	-	Mudstones	9.865761°	34.066018°
KA35	40	9	4,44	--	Evaporite	9.866766°	34.065487°
KA36	25	6	4,17	N175 25 NE	Mudstones	9.866741°	34.065479°
KA37	80	22	3,64	N20 37 E	Mudstones	9.866698°	34.065498°
KA38	100	18	5,56	-	Mudstones	9.866674°	34.065512°
KA39	10	6	1,67	-	Mudstones	9.866799°	34.065442°
KA40	80	15	5,33	-	Evaporite	9.867314°	34.065454°
KA41	10	5	2	-	Mudstones	9.867410°	34.065398°
KA42	12	12	1	-	Evaporite	9.867532°	34.065329°
KA43	10	8	1,25	-	Evaporite	9.867736°	34.065252°